

Hexokinase 1b is a novel target for Non–small-cell lung cancer

Yasemin Yozgat 1,* , Emre Karakoc 2, Ozgur Sahin 3, Seyma Cimen 1,4, Wael M. RabeH 5, Mehmet Serif Aydin 1, Adil Mardinoglu 6,7, Ihsan Gursel 8,9 , Asli Cakir 10 , Ozge Sensoy 1,11 , Ekrem M. Ozdemir 1, Yusuf Bayrak 12 , Mehmet Z. Gunluoglu 13 , Ozge Saatci 3, Javaid Jabbar 14, Juliana C. Ferreira 5, Melike DincceIik Aslan 8, Muzaffer Yildirim 8, Samman Mansoor 1,11, Bilal E. Kerman 15, Zeynep Aladag 1,16, Woonghee Kim 6, Muhammad Arif 6, Emre Vatandaslar 1,17, Olgu E. Tok 1, Zeynep Dogru 18, Asli G. O. Demir 19, Tugce Canavar Yildirim 8 , Ihsan Yozgat 20, Serif Senturk 9, Gurkan Ozturk 1,22, * and Murat Alper Cevher 8,23,*

1 Institute for Health Sciences and Technologies (SABITA), Istanbul Medipol University, Istanbul, Turkey, 34956.

2 Wellcome Trust Sanger Institute, Genome Campus, Hinxton, Cambridge, UK.

3 Department of Biochemistry and Molecular Biology, Hollings Cancer Center, Medical University of South Carolina, Charleston, SC, 29425, USA

4 Department of Nutrition and Dietetics, School of Health Sciences, Istanbul Medipol University, Istanbul, Turkey.

5 Science Division, New York University Abu Dhabi, Abu Dhabi, United Arab Emirates

6 Science for Life Laboratory (SciLifeLab), KTH- Royal Institute of Technology, Tomtebodavägen 23, 171 65 Solna, Stockholm, Sweden

7 Centre for Host–Microbiome Interactions, Faculty of Dentistry, Oral & Craniofacial Sciences, King’s College London, SE1 9RT London, UK

8 Department of Molecular Biology and Genetics, Faculty of Science, Bilkent University, 06800 Ankara, Turkey.

9 Izmir Biomedicine and Genome Center, Izmir, 35340 Balçova, Turkey.

10 Istanbul Medipol University, Faculty of Medicine, Department of Pathology, Istanbul, Turkey.

11 Department of Computer Engineering, School of Engineering and Natural Sciences, Istanbul Medipol University, Istanbul, Turkey

12 Department of Thoracic and Cardiovascular Surgery, Heart and Vascular Institute, Cleveland Clinic Abu Dhabi, Abu Dhabi, United Arab Emirates.

13 Istanbul Medipol University, Faculty of Medicine, Department of Thoracic Surgery, Istanbul, Turkey.

14 Department of Biochemistry and pharmacology, Melbourne University, Parkville, Melbourne, 3010, Australia

15 Departments of Medicine and Neurology, University of Southern California, Los Angeles, California, 90033

16 Department of Medical Biology and Genetics, Institute of Health Sciences, Istanbul Medipol University, Istanbul

17 Department of Histology and Embriology, Istanbul Medipol University, Istanbul, Turkey

18 Department of Biochemistry, Faculty of Medicine, Istanbul Medipol University, Istanbul, Turkey

19 Department of Microbiology, Istanbul Medipol University, Istanbul, Turkey

20 Department of Medical Biotechnology, Institute of Health Sciences, Acibadem Mehmet Ali Aydınlar University, Istanbul, Turkey

21 Molecular Biology Genetics & Bioengineering Program Faculty of Engineering & Natural Sciences, Sabanci University, Orhanli-Tuzla, 34956 Istanbul, Turkey

22 Department of Physiology, School of International Medicine, Istanbul Medipol University, Istanbul, Turkey.

23 Laboratory of Biochemistry and Molecular Biology, Rockefeller University, New York, New York, USA

*To whom correspondence should be addressed. yyozgat@medipol.edu.tr
gozturk@medipol.edu.tr, and murat.cevher@bilkent.edu.tr

The authors declare no potential conflicts of interest

SUMMARY

Deregulation of glycolysis is common in non-small cell lung cancer (NSCLC). Hexokinase (HK) enzymes catalyze the phosphoryl-group-transfer in glucose metabolism. There are a very few studies that have begun to reveal the connections between glucose metabolism and splicing programs. Unlike HK2 gene, which is expressed as a single transcript, there are several transcripts of the HK1 gene due to alternative splicing. However, the functional differential roles of HK1 isoforms in glucose metabolism and tumor progression are still elusive. Here, we show that primary NSCLC patient tumor cells metabolically differ from the normal lung epithelium where they display predominant expression of one of the HK1 transcripts, hexokinase1b (HK1b). We utilized CRISPR-Cas9 system to selectively target specific HK1b isoform in NSCLC and show that silencing HK1b in NSCLC cells inhibits tumorigenesis through diminishing glycolysis and proliferation. Our findings constitute the first demonstration of the first biochemical distinction between the HK1 splice variants. Finally, HK1b deletion sensitizes NSCLC cells to standard-of-care, cisplatin treatment, and the combination therapy synergistically increases both apoptotic cell death by cisplatin and autophagic cell death by increased formation of LC3-II associated autophagic vesicles and myelinoid bodies. Notably, loss of HK1b leads to cellular DNA damage, further combination with cisplatin therapy showed significantly increased levels of DNA damage. Importantly, we showed that glycolysis and cisplatin resistance can be restored by adding-back HK1b in HK1b knock-out cells. Our findings reveal that targeting HK1b isoform alone or in combination with cisplatin may represent a novel strategy for NSCLC patients.

INTRODUCTION

Patients with non–small-cell lung cancer (NSCLC) is often diagnosed with aggressive/metastatic disease which accounts for 85% of all lung cancer, and has limited treatment options¹. NSCLC patients with Kras-activating mutations (10–30%) or loss of function point mutations in p53 (70%) have poor clinical outcomes, and most of the patients eventually relapse following chemotherapy^{30, 73}. Although targeting Kras or modulating p53 expression are attractive therapeutic strategies for NSCLC, attempts to develop drugs that target mutant Kras and convert mutant p53 proteins to a functional state have, so far, been unsuccessful. Only recently, KRASG12C-specific inhibitor sotorasib for NSCLC patients harboring the KRAS p.G12C mutation (13%) received FDA accelerated approval^{23, 63}. Current approaches involve blocking Kras and p53 downstream elements to inhibit NSCLC progression^{12, 65}. Metabolic reprogramming is one of the hallmarks of cancer²¹. Unlike normal cells, cancer cells rely on increased glycolytic flux for their growth and proliferation which renders them more vulnerable to the disruption of glucose metabolism⁷⁰. Although new therapies for targeting altered glucose metabolism showed success in preclinical studies, its application in clinical settings has been limited due to side effects³³. A better understanding of the metabolic dependencies in specific tumor tissues holds the key for exploiting cancer metabolism for clinical benefits and finding a therapeutic option to improve cancer therapy.

Deregulation of glycolysis is common in NSCLC^{9, 18}. Elevated activities of hexokinase were reported in a variety of human cancers^{22, 24, 46}. Hexokinases (HKs) catalyze the essentially irreversible first step of glucose metabolism in cells by phosphorylating glucose to glucose-6-phosphate (G-6-P). The HK enzymes are encoded by four genes, HK1, HK2, HK3, and HK4. While HK1 is ubiquitously expressed in almost all mammalian tissues, HK2 is normally expressed in insulin-sensitive tissues, such as adipose, skeletal, and cardiac muscles. HK3 is usually expressed at low levels while HK4 expression is restricted to pancreas and liver³⁷. Among these, HK1, HK2 and HK3 have a much lower Km value for glucose, suggesting higher affinity for glucose compared to HK4. However, HK1 is the only isoform that shows reduced inhibition by its product G6P in the presence of inorganic phosphate. Therefore, during periods of high energy demand, in which the intracellular concentration of Pi would typically increase while that of G6P decrease, the HK1 activity would increase, causing more glucose being phosphorylated by HK1 and entering downstream metabolism primarily for energy production^{57, 59, 78}. Moreover, both HK1 and HK2 share the most similar structure as they both have N and C-terminal domains, and they both bind the outer mitochondrial membrane *via* a mitochondrial binding domain. Although both HK1 and HK2 have overlapping tissue expression profiles, they have different subcellular distributions. While HK1 is associated mainly with mitochondria, HK2 is associated with both mitochondria and other cytoplasmic compartments²⁶. The association of both HK1 and HK2 with mitochondria is regulated through Protein Kinase B (AKT) and Extracellular Signal-Regulated Kinase (ERK) mediated phosphorylation of Glycogen synthase

kinase 3β (GSK3 β), rendering cells resistant to apoptosis, and is therefore recognized as a key factor for survival of NSCLC cells^{13, 34, 54}.

Compared to *HK2* gene, which is expressed as a single transcript, there are several transcripts of the *HK1* gene due to alternative splicing. According to the RefSeq, there are 10 different isoforms of the *HK1* gene. Half of these isoforms are specific to testis tissue and are not expressed in other tissues^{40, 41}. Here we focused on 3 isoforms with high sequence and structural homology: *HK1a*, *HK1b*, and *HK1c*. Although these transcripts share most of their exons, some of the transcripts have certain exons that can differentiate them from the other transcripts. Importantly, differential expression patterns of *HK1* isoforms (*HK1a*, *HK1b*, and *HK1c*) have not been studied, and their role in NSCLC tumorigenesis, cell survival, and drug response is still elusive. In this line, identification of isoform-specific contributors to cancer cell glucose metabolism that can be selectively targeted to eliminate cancer cells without compromising systemic homeostasis or corresponding metabolic functions in normal cells is a very attractive approach for cancer therapy.

Using cell lines and primary patient tumors/data, we investigated the molecular and functional characterization of HK1 isoforms and demonstrated that HK1b isoform is a critical enzyme in glycolysis metabolism and cell survival. We showed, for the first time, that only HK1b isoform is predominantly expressed in NSCLC cells (A549 WT) and NSCLC patient tumors, and it also distinguishes NSCLC cells from the surrounding normal lung cells. We showed that higher HK1b is associated with poor NSCLC patient survival. In order to identify the mechanisms of HK1b, we deleted HK1b isoform in human NSCLC A549 cells using CRISPR/Cas9 system. Interestingly; HK1b ablation inhibits proliferation and *in vivo* tumor growth of NSCLC cells. Finally, HK1b knock-out in NSCLC cells show sensitization to standard-of-care treatment cisplatin, which in turn, leads to apoptotic and autophagic cell death through the greater induction of DNA damage. Collectively, these findings suggest that therapeutic strategies to modulate the Warburg effect, such as targeting HK1b isoform, may modulate growth and therapeutic sensitivity of NSCLC.

RESULT

HK1 expression is upregulated in human NSCLCs and is associated with poor clinical outcome in patients

To examine the expression of HK1 in human NSCLCs, we analyzed human NSCLC tumor tissues and adjacent non-tumor lung tissues. Pathological details of the patients included in this study are provided in Table 1. We found that in a cohort of patients (13 tumor and 10 adjacent non-tumor samples), both HK1 and HK2 were upregulated in NSCLC tumor tissues as compared to normal lung tissues as indicated with two immunoblotting assays (Fig. 1a and 1b). Quantification of band intensities of HK1 and HK2 revealed that human NSCLC samples have significantly higher HK1 (n=13) ($p<0.001$) and increased HK2 (n=13) ($p=0.037$) expressions (compared to normal tissue) (Fig. 1c), suggesting that HK1 is more ubiquitously overexpressed. We further confirmed the *in-situ* expression of HK1 in NSCLC cells by immunohistochemistry where all the noncancerous epithelium showed weak expression of HK1, while tumor cells showed moderate to strong HK1 expression (Fig. 1d). To investigate the prognostic role of HK1 in NSCLC, we did a survival analysis which showed that higher expression of HK1 was associated with decreased relapse-free survival ($p=0.01$; Figure 1e). This suggests that elevated HK1 expression is associated with worse disease progression.

Human NSCLC cells express one of the HK1 isoforms- hexokinase1b (HK1b) which is a poor prognostic factor

The HK1 gene spans approximately 131 kb and consists of 25 exons. According to RefSeq, alternative splicing of *HK1* gene at its 5' end produces different transcripts in different cell types. The testis-specific exons are located at approximately 15 kb upstream of the erythroid-specific exon R. The first 5 exons of the *HK1* gene encode for the testis-specific sequences. The 6th exon is the erythroid-specific exon R⁴¹. When these tissue specific transcripts are excluded, 3 remaining transcripts are; *HK1a*, *HK1b* and *HK1c*. On the other hand, the *HK2* gene has one transcript in the RefSeq (Supplementary Fig. S1a). Although there are a few studies on the testis specific transcripts⁴⁰, the differential expressions of three non-tissue specific *HK1* isoforms in different tissues (including the cancer tissues) and their functional role has not been reported. When we analyze the *HK1* transcripts, it is possible to differentiate them using the differentially used exons. *HK1a* transcript contains different exons at the 5' end, and therefore it is possible to distinguish this transcript. Both *HK1b* and *HK1a* isoforms possess one extra exon, exon 8, which is missing in the *HK1c* isoform. Using these exon-exon junctions around exon 8, we were able to design specific genomic probes to differentiate *HK1b* and *HK1c* isoforms. Overall, designing specific primers for these exons allow us to quantify the expressions of these isoforms. Moreover, the extra exon in *HK1b* codes for 32-amino acid long alpha-helix that is part of the small sub-domain (Supplementary Fig. S1b).

We first analyzed *HK1a*, *HK1b*, and *HK1c* isoforms along with *HK2* and p53 as a control in NSCLC adenocarcinoma cell line (WT-A549). A549 does not express *HK1a* isoform, but it expresses *HK1b* isoform and *HK2* predominantly while *HK1c* isoform is expressed at low level shown by semi-qPCR (Fig. 2a). Importantly, to evaluate the clinical relevance of *HK1b* upregulation in human NSCLC, we performed semi-qPCR and qRT-PCR analyses on tumors and adjacent non-tumor samples from NSCLC patients. In particular, *HK1b* expression was significantly ($p=0.005$) higher in the NSCLC tumor when compared to normal adjacent tissue ($p=0.005$). Moreover, *HK2* ($p=0.03$) and p53 ($p=0.005$) expressions were also increased in the NSCLC tumor when compared to normal adjacent tissue (Fig. 2b and 2c). *HK1c* isoform expression was not significantly different between normal and tumor tissues, supporting the idea that *HK1b* was uniquely upregulated in comparison to *HK1c* isoform and *HK2* in NSCLC. In addition, NSCLC patient tumor cells showed no *HK1a* isoform expression (Fig. 2b).

In order to further validate the increased expression of the *HK1b* isoform between the NSCLC adenocarcinoma and the normal lung tissues, we merged the most extensive public databases TCGA (The Cancer Genome Atlas) Project and the GTEx (Genotype-Tissue Expression) Project. TCGA Lung Adenocarcinoma project contains RNA sequencing of 426 lung tumor tissues. These tumor samples, adenocarcinoma ($n = 511$) and squamous cell carcinoma (SCC) ($n = 501$), are matched with 602 normal lung tissues from the GTEx Project. Consistent with RT-PCR analyses, the comparison of the expression of the *HK1b* isoform (transcript variant-8) between normal and TCGA Lung adenocarcinoma samples (RefSeq id NM_001322366) showed a significant upregulation of *HK1b* in NSCLC tumor tissues compared with those in normal lung tissues ($p= 1.85e-07$) (Fig. 2d). Altogether, these data reveal that elevated *HK1b* expression is specific to NSCLC across a wide selection of lung cancer patients when compared to normal lung tissues. Moreover, higher expression of the *HK1b* isoform is associated with decreased survival probability for both adenocarcinoma (Fig. 2e) and squamous cell carcinoma (Fig. 2f) types of NSCLC, albeit the latter is not significant ($p= 2.7e-02$, $p=9.5e-02$, respectively). Collectively, our data provide compelling evidence for the specificity of *HK1b* isoform in NSCLC, which may be an attractive therapeutic target.

Deletion of *HK1b* suppresses cell proliferation and tumorigenesis in NSCLC cells *via* regulating glycolytic activity.

To understand the specificity of *HK1b* role in NSCLC oncogenesis, we utilized CRISPR/Cas9 system to genetically disrupt *HK1b* isoform in A549 cells and obtained isogenic cell lines, as described previously⁵³. Single-cell clones expressing sg*HK1b* were screened for *HK1b* isoform elimination at the expense of specific indel mutation generation at target loci. PCR and DNA fragmentation analyses showed deletion of 14 bp nucleotides in *HK1b*, resulting in a frame-shift mutation (Supplementary Fig. S2a). We further analyzed isogenic clones expressing sg*HK1b* with qRT-PCR. Of note, we were able to delete *HK1b* isoform specifically without altering the transcriptional expressions of *HK1c* isoform and *HK2* (Fig. 3a). Semi-q-PCR data of A549 WT,

A549 HK1b^{-/-} (Fig. 3a) and as a control H1299 cells (Supplementary Fig. S2b) confirmed the deletion HK1b isoform. Moreover, immunofluorescence and immunoblot analyses confirmed that HK1 protein was absent due to permanent loss of HK1b isoform (Fig. 3b and 3c).

To test the role of HK1b isoform in tumorigenesis, we performed both subcutaneous and intra-tracheal xenograft models of lung cancer. An intra-tracheal lung tumor model was generated where A549 WT and A549 HK1b^{-/-} cells were implanted into immunodeficient NSG male mice *via* intra-tracheal injection. Mice were sacrificed at 8 weeks post-implantation, and the relative tumor volumes were measured. Tumor size was significantly reduced in mice bearing A549 HK1b^{-/-} cells compared to control ($p=0.01$) (Fig. 3d). As a second model subcutaneous lung tumor model was generated where mice were injected with A549 WT and A549 HK1b^{-/-} cells subcutaneously in the lower right flank of mice, and tumor volume was measured over a period of 56 days from the day of injection. Tumor size was significantly reduced in mice bearing A549 HK1b^{-/-} cells compared to control (Fig. 3e). Histopathological evaluation of A549 WT or A549 HK1b^{-/-} tumors in both models confirmed that they are both NSCLC lung adenocarcinomas. HK1 staining confirmed almost complete depletion of HK1 expression in A549 HK1b^{-/-} tumors, while A549 WT tumors expressed high levels (Supplementary Fig. S3a and S3c). Furthermore, in both models, *in situ* analyses of tumor tissues showed significantly lower Ki-67 staining in A549 HK1b^{-/-} tumors compared to control tumors ($p=0.001$), albeit the A549 HK1b^{-/-} tumors showed higher significant reduction of Ki-67 positivity in subcutaneous model ($p=0.001$) (Supplementary Fig. S3b and S3d), indicating that HK1b KO cells have less proliferation ability.

We then analyzed the metabolic consequences of HK1b isoform deficiency. Changes in glycolysis and respiration were measured using the Seahorse metabolic analyzer. Analysis of the mitochondrial respiration rate following HK1b knockout (KO) resulted in nonsignificant changes in oxygen consumption rate (OCR) and basal respiration (Fig. 3f), suggesting that HK1b ablation did not alter the mitochondria-driven oxidative phosphorylation (OXPHOS). However, measuring extracellular acidification rate (ECAR) showed significant reductions in glycolytic activity in A549 HK1b^{-/-} when compared to A549 WT ($p=0.0001$) (Fig. 3g). To investigate whether WT HK1b-forced expression restores glycolysis, A549 HK1b^{-/-} cell lines stably expressing HK1b fused with eGFP was established (A549 HK1b^{-/-} +HK1b). Approximately by 80% of glycolysis (ECAR) was restored by re-expressing WT HK1b in A549 HK1b^{-/-} cells (Figure 3h). HK1 is known to localize to mitochondria via association with VDAC at the mitochondrial outer membrane⁵⁷. Immunofluorescent staining illustrated that the majority of WT HK1b expression in into A549 HK1b^{-/-} cells resulted in strong GFP signal emissions that colocalized with Mito Tracker Red stained mitochondria, whereas no GFP fluorescence was detected with the corresponding empty plasmid in control cells (A549 WT and A549 HK1b^{-/-})(Fig. 3i).

In order to evaluate the effect of reduced glycolysis on proliferation *in vitro*, flow cytometry analyses of Ki67 was performed and A549 HK1b^{-/-} cells showed an approximately 35% decrease in Ki-67 positivity (Fig. 4a). In order to demonstrate the clinical relevance of the lack of HK1b

expression and rates of glycolysis and clinical outcome, we performed RNA-sequencing of A549 WT and HK1b^{-/-} cells, and generated a HK1b knockout (HK1b KO) signature comprising the most differentially expressed 514 genes upon HK1b knockout (p-adjusted<0.001, Supplementary Table S2). The clinical relevance of our HK1b KO signature was first tested based on the differential expression in normal lung vs. lung adenocarcinoma tissues, and a significantly lower HK1b KO signature score, i.e. high HK1b expression, was observed in two different patient datasets (GSE10072²⁸ GSE32863³²) (Fig. 4b), in line with our previous data (Figures 1a-d). Gene set enrichment analysis demonstrated that glycolysis-related genes were enriched among lung cancer patients from GSE101929³⁹ with low HK1b KO signature score, i.e. those who have high HK1b levels (Fig. 4c). Furthermore, the enrichment of oxidative phosphorylation-related genes among the same patients were a lot weaker (p-value<0.001 versus p-value=0.041), supporting our hypothesis that HK1b specifically controls glycolysis (Fig. 4d). Most importantly, separating lung adenocarcinoma cancer patients from TCGA (<https://www.cancer.gov/tcga>) based on the levels of HK1b KO signature score revealed a significantly higher overall survival in patients having a high HK1b KO signature score, i.e. patients who are predicted to express low levels of HK1b (Fig. 4e). In conclusion, all these data show that inhibition of HK1b reduces cell proliferation and tumor cell growth in NSCLC which may be attributed to the reduced glycolysis.

Although HK1b, c and HK2 have structural similarities, major differences in their N-terminal sequences distinguish each from one another and thus provide distinct biochemical and functional properties in glycolytic pathway and tumor development^{17, 49, 58, 60}. Thus, we next investigated whether the structural difference between HK1b and HK1c is the major contributor to the phenotypic changes that were observed in A549 WT cells upon HK1b loss. N-terminal domains stabilize HK1 and HK2 enzymes and are involved in their binding to the outer mitochondrial membrane^{2, 58}

We first explored the effect of the structural difference between dynamics of HK1b and HK1c isoforms using root-mean square fluctuation (RMSF) and biochemistry analysis. The HK1c isoform compare to the other human enzyme is missing 32 amino acids from residues A166 to G197. Computer simulation revealed the deletion of the 32 amino acids in the small subdomain of N-terminal domain of HK1c isoform might lower its thermodynamic stability and HK1b isoform displays relatively less fluctuation compared to HK1c isoform and HK2 as shown by RMSF analysis (Fig. 5a). To confirm these observations, the HK1b and HK1c isoforms were expressed and purified to >95% purity with purification yield of HK1c 3-folds lower than HK1b (Fig. 5b). The secondary structure of both isoforms was intact according to circular dichroism scans and were similar to human HK2⁴² (Fig. 5c). As predicted by Molecular Dynamics simulations, the thermodynamic stability of the HK1c isoform was compromised based on the thermograms generated by differential scanning calorimetry (DSC) (Fig. 5d). The presence of 5 mM glucose had negligible effect on the stability of HK1c, which increased the stability of HK1b isoform. The loss of HK1c ability to adapt a thermodynamically stable glucose

conformation is due to the deletion in its N-terminal domain. Similar effect has been shown in HK2, where N-terminal domain is important for the stability of the full enzyme⁴². The relative enzymatic rate of HK1c was 40% of the HK1b isoform, and initial velocity studies further confirmed that the catalytic rate of HK1c was 2.5-fold lower with V/E_t of 2.8 s^{-1} compare to 6.9 s^{-1} for HK1b (Fig. 5e and 5f). Both HK1 isoforms are active at the C-terminal domain, and even though the amino acid deletion of HK1c is at the N-terminal domain, it still affected the C-terminal domain activity. Overall, the HK1b isoform is thermodynamically more stable and catalytically more efficient than the HK1c isoform. Consequently, this may impact the strength of the interaction between mitochondria and HK1b as this helix was shown to be at interface of mitochondria and the HK1b thereby may result change in glycolytic activity⁵⁸.

HK1b plays critical role in cisplatin response, metabolism, and survival in NSCLC cells

Chemotherapy is often one of the first line therapies in NSCLC patients. Cisplatin is slightly more effective platinum-based treatment for NSCLC patients. However, patient may show *de novo* or acquired resistance to cisplatin, and also cisplatin has been associated with wide range of side effects^{11, 45}. We first investigated whether the HK1b deletion could sensitize NSCLC cells to cisplatin treatment. Cell viability assays which were performed in A549 HK1b^{-/-} cells showed significantly lower IC50 value for cisplatin ($47\mu\text{M}$) than the A549 WT control group ($75\mu\text{M}$) (Fig. 6a). Based on these results, A549 WT and A549 HK1b^{-/-} cells were treated with cisplatin at $75\mu\text{M}$, for 48 hours. Flow cytometric quantification of apoptosis measured by double Annexin V-FITC and PI propidium iodide (PI) staining. HK1b deletion when combined with cisplatin treatment significantly augmented apoptotic cell death in A549 HK1b^{-/-} cells (Fig. 6b) (from 33% to 81 %). To further demonstrate the specific effect of HK1b on cisplatin resistance, we did a rescue experiment by overexpressing HK1b in A549 HK1b^{-/-} cells (A549 HK1b^{-/-} +HK1b). Cell viability assay which was performed in A549 HK1b^{-/-} +HK1b cells showed significantly higher IC50 value for cisplatin ($147\mu\text{M}$) than both control groups of A549 WT ($80.8\mu\text{M}$) and A549 HK1b^{-/-} ($46.7\mu\text{M}$) (Fig. 6g). We then analyzed expression level of HK1b using semi-qPCR, which was higher in A549 HK1b^{-/-} +HK1b cells than in A549 WT cells and was absent in A549 HK1b^{-/-} cells (Fig. 6h). Our result showed that increased levels of HK1b expression were correlated with levels of resistance to cisplatin.

We found that cisplatin treatment induces cleavage of PARP and caspase 3, but induction of cleavage was significantly higher in A549 HK1b^{-/-} cells (Fig. 6c, Supplementary Fig. S4a). Interestingly, HK1b deletion slightly induces down-regulation of anti-apoptotic Bcl-2 protein and up-regulation of pro-apoptotic Bax protein expressions in untreated A549 HK1b^{-/-} cells and further downregulation of Bcl-2 and up-regulation of Bax expressions was significant with the cisplatin treatment (Fig. 6c, d, and Supplementary Fig. S4a). Altogether, these results suggest that loss of HK1b sensitizes NSCLC cells to cisplatin by inducing apoptosis.

In order to identify the underlying molecular mechanisms of increased apoptosis induction upon HK1b loss under cisplatin treatment, we examined signaling pathways. It was previously

reported that cisplatin induces ERK activation leading to p53 phosphorylation (Ser 15) and stabilization and DNA damage⁵⁰. It was also shown that GSK3 beta is phosphorylated (Ser 9) and inactivated by Erk, leading to apoptosis. Upon silencing of HK1b, phosphorylation of both Erk1/2 and GSK3 beta increased. This was accompanied by increased p53 phosphorylation. Importantly, phosphorylations of ERK, GSK3 β and p53 are further increased by cisplatin treatment, especially in A549 HK1b^{-/-} cells (Fig. 6e, f, and Supplementary Fig. S4b). These results show that HK1b is involved in cisplatin induced DNA damage, activating ERK signaling and leading to phosphorylation of GSK3 beta and p53 culminating in apoptosis.

Depletion of HK1b sensitizes cells to cisplatin induced cytotoxicity via autophagic cell death and higher induction of DNA damage.

Since HK1b deletion results in glycolysis reduction and synergizes cells to cytotoxic cell death, we investigated the underlying mechanism of apoptotic cell death in HK1b deleted cells upon treatment with cisplatin. Recent reports suggest a complex and multifaceted relationship between autophagy and apoptosis. Moreover, glucose deprivation typically results in autophagy induction to maintain energy homeostasis¹⁴. However, autophagy might be growth inhibitory after a certain threshold³⁶. In order to determine whether the combination of HK1b deletion and cisplatin led to the activation of autophagy in NSCLC cells, we examined the markers of autophagic signaling pathway upon treatment with cisplatin. HK1b elimination induces autophagy in response to glucose deprivation since formation of LC3II significantly elevated in A549 HK1b^{-/-} cells. Moreover, expression of the autophagy marker LC3-II was markedly induced in HK1b deleted cells when treated with cisplatin (Fig. 7a). Furthermore, cisplatin inhibits phosphorylation of mTOR in A549 HK1b^{-/-} cells (Fig. 7a). In order to demonstrate the clinical relevance of the induction of autophagy, we performed GSEA in patients from GSE101929 and observed enrichment of autophagy-related gene sets among patients with high HK1b KO signature score, i.e., patients with low HK1b (Fig. 7c). We further demonstrate that cisplatin treatment induces significant numbers of autophagic vesicles and myelinoid bodies in HK1b deleted cells as demonstrated by electron microscopy (Fig. 7e). Indeed, it was shown that cisplatin induced not only apoptosis but also autophagy and ER stress in lung cancer cell lines⁶². These data imply that combination of HK1b deletion with cisplatin induces greater cell death through increased activity of autophagy induced apoptosis.

Recent studies suggest a link between DNA repair and glycolysis^{43, 64, 69}. To investigate whether the glucose deprivation as a result of HK1b depletion induces DNA strand breaks (DSBs), we analyzed the activation of H2AX in both untreated and cisplatin-treated cells (A549 WT and A549 HK1b^{-/-} cells). Indeed, DSBs are highly toxic lesions, with a single unrepaired DSB being sufficient to trigger cell death⁶⁸. Interestingly, a loss of HK1b resulted induction of H2AX in A549 HK1b^{-/-} cells (p-value \square 0.001) (Fig. 7a, b). Moreover, combination of HK1b deletion and cisplatin could further increase the level of DNA damage in A549 HK1b^{-/-} cells, the phosphorylation level of H2AX (Ser139), was markedly elevated after cisplatin treatment (p-value \square 0.001) (Fig. 7a, b, and Supplementary Fig. S4c and d). In line with our previous data

with greater cell death in A549 HK1b^{-/-} cells, altogether our data indicate that loss of HK1b may potentiate cisplatin-induced DSBs. Importantly, gene sets related to DNA repair were enriched among patients with low HK1b KO signature score, i.e., patients with high HK1b, suggesting that a high expression of HK1b might promote DNA repair and confer resistance against DNA damaging agents (Fig. 7d). These results show that disrupting cancer metabolism by depleting HK1b revealed roles for glycolysis in promoting DNA repair response and indicating that HK1b is a critical mediator in between DNA repair and glycolysis pathways.

DISCUSSION

Like most cancers, NSCLC display comprehensive multiple metabolic alterations, such as reprogramming of glucose metabolism and increased dependency on glycolysis^{31, 51}. This is manifested by turning on the expression of certain enzymes, such as Hexokinases (HKs) that are required for the accelerated glucose metabolism in NSCLC cells. Selective HK isoforms that regulate glucose metabolism in NSCLC cells but dispensable or absent in normal lung cells would be an attractive molecular target for cancer therapy. Here we demonstrated that HK1 expression was significantly elevated in comparison to HK2 expression in NSCLC patient tumor samples.

It is known that alternative splicing of HK1 gene results in several transcripts encoding different isoforms according to RefSeq. We analyzed the expression of 3 different isoforms of HK1 (HK1a, b, and c) in NSCLC cells and primary tumor tissues. We found that HK1b isoform was predominantly expressed in A549 NSCLC cells. Importantly, significantly elevated HK1b isoform in patient tumors as compared to normal tissue has also been detected, indicating a higher dependency on glycolysis and resistance to cell death in these tumor cells. In addition to these, the results from our survival analysis using TCGA datasets clearly demonstrated that high HK1b expression levels were associated with poor clinical outcomes in patients with NSCLC. Our data suggests that HK1b isoform may have therapeutic utility targeting metabolic pathway in NSCLC.

To extent the clinical relevance of HK1b, we examined the functional role of HK1b by deleting HK1b isoform in A549 cells using CRISPR/Cas9 system. We found that HK1b deletion inhibits proliferation and tumorigenesis *in vivo*. Indeed, malignant cells support tumor proliferation and progression by adopting to metabolic changes²⁹. Our metabolic analysis of HK1b KO resulted significantly reduced glycolysis of NSCLC cells. Furthermore, our results provide experimental evidence for this hypothesis by showing that HK1b can fully restore ECAR to almost the same level of WT HK1b, supporting a unique role of HK1b in NSCLC growth. To further understand the biological functions of HK1b KO in NSCLC cells, we characterized their transcriptional profiles in comparison to isogenic control NSCLC cells using RNA-seq, and widespread changes (514 most differentially expressed genes) were observed upon HK1b KO. In our study, GSEA analysis was carried out based on the RNA seq data, showed a significant correlation between HK1b isoform expression and signatures representing the glycolytic phenotype. Moreover, application of HK1b KO signature in the clinical setting showed that high HK1b expression was observed in two different patient datasets. Importantly, we were able to show statistically significant clinic relevance between HK1b expression and unfavorable prognostic gene signature by applying the levels of HK1b KO signature score on lung adenocarcinoma patients from TCGA. The level or gene signature of HK1b expression could potentially be used as a prognostic factor in NSCLC.

Importantly, HK1b deletion synergizes with cisplatin to sensitize NSCLC cells to cell death because of significant reduction of glycolysis and downregulation of the anti-apoptotic proteins. Notably, enforced expression of HK1b in A549 HK1b^{-/-} cells induce greater resistance to cisplatin significantly more than even parental A549 WT cells. Indeed, HK1 was found to have role in blocking apoptotic signals through antagonization of pro-apoptotic Bcl-2 proteins at mitochondria⁶⁰. The treatment options for NSCLC patients are based mainly on several factors, including the stage of the cancer and availability of molecular markers for targeted therapy. Currently, cisplatin is widely used as one of the main platinum-based drugs, but low efficacy and considerably side effects as a single agent would not benefit NSCLC patients¹¹. Our results provide first evidence that the combination of cisplatin and HK1b silencing markedly increased NSCLC cell death. The mechanism by which HK1b deletion synergizes cells to cisplatin cytotoxicity may be through blocking its binding ability to mitochondria. Our work is consistent with the previous report, suggesting that the increased expression of HK1 attenuates apoptosis in a glucose-dependent manner because of its anti-apoptotic effect and also induction of increased HK activity¹⁹. As previously reported, mitochondrial binding of HKs near voltage-dependent ion channel (VDAC) may be required for access to ATP to efficiently phosphorylate glucose⁸.

Furthermore, we showed that N-domain of HK1b isoform is more stable around the glucose and ATP binding site compared to HK1c isoform and HK2 using molecular dynamic simulations. Moreover, we found HK1b isoform is thermodynamically more stable and catalytically more efficient than the HK1c isoform using biochemistry analysis. Our findings are in agreement with previous studies that HK1 has much higher strong binding affinity for VDAC1 than HK2 has^{26, 76, 79}. Therefore, our result might provide a better explanation for higher stability of HK1b over HK1c isoform and HK2 by showing that HK1b deletion induces significant depletion of glycolysis. Moreover, HK1b ablation alone or with cisplatin increases ERK, and GSK3 β signaling. ERK has role in promoting glycolysis^{47, 55}. ERK increases glycolysis by upregulating transcriptional expressions of several metabolic genes^{7, 80}. ERK activation phosphorylate GSK3 β (Ser9) and resulting its inactivation in an AKT independent manner^{13, 54}. The inhibition of GSK3 β (Ser9) is required for the stimulation of glycogen and protein synthesis and, was also suggested as a mechanism for increased resistance to apoptosis of cancer cells¹⁶. Recent studies strongly indicate that mitochondrial-bound HK1 and HK2 play a major role in preventing tumor apoptosis by blocking mitochondrial outer membrane permeabilization (MOMP) and the association is regulated by GSK3 β ^{48, 60}. Here, we found that synergetic effect of HK1b ablation and cisplatin induces higher activation of ERK and inhibition of GSK3 β because of significant reduction in glycolysis. It was suggested that, cisplatin induces DNA damage thereby activates ERK, and extensive DNA damage-induced by ERK activation causes apoptosis^{66, 75}. Importantly, we demonstrated that ablation of HK1b induces DNA damage, and the damage further increases with cisplatin treatment. Similarly, GLUT inhibitor phloretin has been demonstrated to increase phosphorylation of JNK, p38, and ERK in breast tumor cells and NSCLC cells by enhancing the DNA damaging^{38, 77}. Furthermore, we showed downregulation of

anti-apoptotic Bcl-2 upon HK1b deletion which was further reduced by cisplatin treatment. On the contrary, we showed upregulation of pro-apoptotic Bax upon HK1b deletion which was further increased by cisplatin treatment. These results suggest that HK1b has an important role in not only glycolysis but also apoptotic resistance mechanism.

Several studies have reported that enhanced aerobic glycolysis confer cancer cells resistance to cisplatin through both decreased signatures of DNA damage and upregulated DNA recombination competence⁴. In a cisplatin-resistant gastric cancer cell model, glycolysis levels were shown to be significantly increased. Gastric cancer cells were significantly more sensitive to cisplatin after the inhibition of glycolysis via treatment with 2-deoxy-D-glucose, a glucose-competitive substrate^{52, 72}. Govoni et al. have reported that lactate, the product of LDH reaction in final step of glycolysis, causing intrinsic resistance of cancer cells to cisplatin through upregulated expression of DNA repair genes²⁰. In line with previous studies, we demonstrated that HK1b might promote DNA repair and confer resistance against DNA damaging agents. We showed that deletion of HK1b induces phosphorylation of H2AX in Ser139 and the activation was further increased with cisplatin treatment in A549 HK1b^{-/-} cells. Furthermore, we were able to demonstrate the clinical relevance of the induction of DNA damage response, we performed GSEA in patients from GSE101929 and observed enrichment of DNA repair -related gene sets among patients with low HK1b KO signature score, indicating that HK1b may promote drug resistance through upregulation of DNA repair genes. Although we were able to link glycolysis and DNA repair by demonstrating the role of HK1b in upregulation of DNA repair pathways, underlying mechanism is still unclear. However, several studies have provided some insights into functional links between glycolysis, autophagy and DNA repair pathway^{15, 71}. It has been reported that inhibition of ENO1 could induce autophagy to arrest cellular growth⁶. Kang et al. have reported that activation of autophagy contributes to DNA damage-induced senescence²⁷. In line with previous studies we were able to show induction of autophagy as a result of HK1b deletion. Altogether our data have suggested inhibition of glycolysis by HK1b deletion induce autophagy and DNA damage, indicating the key role of HK1b in cancer therapy resistance.

Recent studies have showed that there is a regulatory relationship between autophagy and glycolysis and HKs has role in mediating this switch.²⁵ It was reported that HK2 has role in regulating the switch from glycolysis to autophagy during nutrient starvation through mTOR complex 1 (TORC1) inhibition in heart⁵⁶. It was also demonstrated that HK1 is a direct substrate of the autophagy-initiation kinases ULK1/2, which sustains glycolysis under certain circumstances. To determine whether HK1b plays a regulatory role in autophagy under glucose deprivation, we evaluated NSCLC cells after ablation of HK1b and determined the possible change with cisplatin treatment. We found that HK1b deletion induces autophagy in A549 HK1b^{-/-} cells with increased *LC3B-II* formation as well as mTOR inhibition. We also observed that autophagy was significantly elevated in A549 HK1b^{-/-} cells in combination with cisplatin at multiple levels. Furthermore, electron microscopy images revealed significantly increased numbers of autophagic vesicles and myelinoid bodies in HK1b deleted cells upon cisplatin

treatment. Our results suggest that HK1b has a role in mediating glycolysis and the autophagy. Indeed, we showed that ERK was activated upon HK1b deletion and activation further increased in combination with cisplatin treatment. In line with our results, several studies have shown that ERK has role in not only regulating glucose metabolism but also in mediating autophagy of highly proliferating cells in cancer^{35, 47}. Moreover, several studies have shown that glycolysis regulates autophagy and plays a key role in chemo-resistance in cancer¹⁰. It was reported that hexokinase 2 (HK2) conferred resistance to cisplatin in ovarian cancer cells by increasing ERK1/2 phosphorylation as well as autophagic activity⁸². Later studies with ovarian cancer cells have revealed that cisplatin induce autophagy through activation of ERK1/2^{3, 74}. Taken together, our studies provide first evidence that HK1b is a compelling metabolic therapeutic target that may also potentiate the efficacy of cisplatin in NSCLCs.

MATERIAL AND METHODS

Cell culture and treatment

Human non–small cell lung cancer (NSCLC) cell lines, including A549, H1299, were obtained from Dr. Engin Ulukaya's laboratory (University of Istinye) and propagated in monolayer culture in RPMI 1640 supplemented with 10% FBS, 1% penicillin–streptomycin, and 1% L-glutamine. All cells were maintained in a humidified atmosphere containing 5% CO₂ at 37°C. All cell lines were tested for Mycoplasma routinely every 3 months using MycoProbe Mycoplasma Detection Kit (R&D Systems).

Chemicals, antibodies and reagents

Rabbit monoclonal primary antibodies against HK1 (C35C4), HK2 (C64G5), Cleaved PARP (Asp214) (D64E10), Cleaved Caspase-3 (Asp175) (5A1E), Caspase-3 (D3R6Y), Bax (D2E11), Phospho-GSK-3 β (Ser9) (D85E12), total GSK-3 β (D5C5Z), Phospho-p53 (Ser15), Phospho-mTOR (Ser2448) (D9C2), Phospho-p44/42 MAPK (Erk1/2) (Thr202/Tyr204) (D13.14.4E), p44/42 MAPK (Erk1/2) (137F5), β -Actin (13E5), GAPDH (D16H11) and horseradish peroxidase (HRP)-conjugated rabbit and mouse secondary antibodies for immunoblot and MitoTracker Red CMXRos for immunofluorescence purchased from Cell Signaling Technologies (USA). Mouse monoclonal primary antibodies against p53 (DO-1), Bcl-2 (C-2), and MAP LC3 β (G-2), purchased from Santa Cruz Biotechnologies (USA), and Anti-phospho-Histone H2A.X (Ser139) Antibody, clone JBW301, purchased from Millipore. Cisplatin (50 mg/100mL) was purchased from Koçak Farma. Cell culture medium (RPMI-1640), FBS, glutamine, penicillin, and streptomycin were acquired from Gibco (Grand Island, NY).

Gene knockout in lung cancer cells

A549–HK1b isoform-knockout cells were generated by using the CRISPR/ Cas9 genome editing system. Briefly, the sgRNAs specific for *HK1b* isoform only was designed to target the 8th exon of human *HK1* gene. pX458 vector with GFP selection marker from Addgene, as described previously⁵³, was used to deliver Cas9 and a sgRNA targeting *HK1b* (namely sgHK1b) into the target cells. The expression of single-cell clones expressing sgHK1b were screened for HK1b isoform elimination and specific indel mutations at target loci was confirmed with PCR, DNA fragmentation analyses. The CRISPR guide sequences targeting *HK1b* were sense: GCGATTTAAAGCGAGCGGAG, antisense: CTCCGCTCGCTTTAAATCGC

Cloning and Lentivirus production

For the lentiviral expression of HK1b-GFP (GenScript), the sequence was cloned into the pCSC-SP-PW-GFP lentiviral backbone (A kind gift from Fred Gage). pBOB-GFP plasmid was digested with MssI and XbaI restriction enzymes to remove the GFP sequence and was dephosphorylated. HK1b-GFP sequences were amplified by PCR with the use of forward (5' TTTCTAGATATGATCGCCGCG 3') and reverse (5'TTGTTTAAACTTTTACTTGTAC AGCTC 3') primers. After gel isolation, vector and insert were ligated at 1:3 ratio by using

ThermoFisher ligation kit (K1423). Next, 5 μ l of the ligation product was transformed to Stbl3 bacteria using heat shock method. Next day, single colonies were picked to verify cloning. Lentiviruses were produced as described previously⁶⁷.

Cell viability assay

Twenty-four hours following seeding (15,000 cells/well) in a 96-well plate, A549 and A549 HK1b^{-/-} cells were treated with vehicle (*phosphate buffered saline*), or cisplatin (0.9% NaCl w/w) with concentrations ranging from 0–100 μ M/ml and the cells were incubated for a further 48 h. The cell viability was determined using the CellTiter-Blue assay kit (Promega) according to the manufacturer's instructions. IC₅₀ was defined as the concentration causing a 50% reduction in absorbance relative to the negative control. IC₅₀ was determined by non-linear regression analysis using Graphpad Prism v8 (Graphpad Software, CA, USA). IC₅₀ concentration of cisplatin are used in A549 (75 μ M) and A549 HK1b^{-/-} (47 μ M) cells and after 48hrs treatment cells were harvested by trypsinization, collected by centrifugation, washed once with 1 ml of PBS and stained with propidium iodide (BD Biosciences) according to the manufacturers' protocol and number of death cells was measured using fluorescence-activated cell sorting.

RNA isolation and quantitative PCR

RNA was isolated from human NSCLC cells and human clinical NSCLC tumor and normal samples by homogenization in Trizol reagent (Invitrogen) according to the manufacturer's instructions, followed by purification on an RNeasy column (Qiagen). RNA purity was assessed by Thermo NanoDrop 2000 (Thermo Fisher Scientific, Inc.) by standard absorbance ratios as A₂₆₀/A₂₈₀ \geq 1.8 and A₂₆₀/A₂₃₀ \geq 1.5. Complementary DNAs were synthesized from 2 μ g of total RNA using RevertAid First Strand cDNA Synthesis Kit (Thermo Fisher Scientific, Inc.) Real time Quantitative PCR (RT-*qPCR*) results obtained with *Bio-Rad's* iTaq Universal SYBR Green Supermix.. The threshold cycle (Ct) for individual reactions were identified using iCycler IQ sequence analysis software (Bio-Rad). β -actin was used for normalization of the data. All experiments were performed in triplicate. The following primers were used in this study with the following sequences:

HK1a isoform	Fwd., 5'- TGCCAAGCCCTGTTCTATGC -3'
	Rev., 5'- GCTGGGTCTTGAACGCACTG -3'
HK1b isoform	Fwd., 5'- CGCTGAAGACCCAGATTGACA -3'
	Rev, 5'- GCACCCGCAGAATTTCGAAAG -3'
HK1c isoform	Fwd, 5'- GCTGAGTGCCTGGGAGATTT -3'
	Rev., 5'- TGGCATCATAGTCCTCATCTATTT -3'
HK2	Fwd, 5'- CAACTTCCGTGTGCTTTGGG -3'
	Rev., 5'- TGAGACCAGGAACTCTCGT -3'
p53	Fwd, 5'- GGAGCACTAAGCGAGCACTG -3'
	Rev., 5'- TCTCGGAACATCTCGAAGCG -3',
H ₂ O	Fwd, 5'- AGAGCTACGAGCTGCCTGAC -3'
	Rev., 5'- AGCACTGTGTTGGCGTACAG -3'

RNA sequencing

Total RNA (50 µg) for the human A549 HK1b KO and A549 WT cell lines was used to generate whole transcriptome libraries for RNA sequencing and the library were prepared with Illumina TruSeq Stranded mRNA with Poly-A selections. Clustering was done by 'cBot' and samples were sequenced on NovaSeq6000 (NovaSeq Control Software 1.6.0/RTA v3.4.4) with a 2x51 setup using 'NovaSeqXp' workflow in 'S1' mode flowcell. The Bcl to FastQ conversion was performed using bcl2fastq_v2.20.0.422 from the CASAVA software suite. The quality scale used is Sanger / phred33 / Illumina 1.8+.

The raw RNA sequencing data were processed with Kallisto (PMID: 27043002)⁵ with index file generated from Ensembl Reference Genome (PMID: 29155950)⁸¹. The outputs were then grouped on the gene level and estimated count were rounded to get integer value. We performed differential gene expression analysis using DESeq2 (PMID: 25516281) and functional analysis using PIANO (PMID: 23444143). Gene-set collections for PIANO were retrieved from Enrichr (PMID: 27141961). All the analyses were performed in RStudio.

Western blot analysis

Cells were harvested and subjected to lysis buffer (25 mM Tris-HCl pH 7.4, 150 mM NaCl, 1% NP-40, 1 mM EDTA, 5% glycerol, 25 mM NaF), containing proteinase inhibitor cocktail and phosphatase inhibitor cocktail (Roche) and then subjected to sonication for total lysates recovery. The lysates were subjected to centrifugation at 10,000 g at 4C for 20 minutes and the supernatants removed. The total protein (50 µg) was fractioned by 10% SDS-PAGE and electrophoretically transferred to Immobilon-FL PVDF membranes. The membrane was blocked with blocking buffer (Li-Cor) at room temperature for 1 hour, and then incubated with appropriate primary antibody at 4C overnight. After washing with PBS containing 0.05% Tween 2 (PBST), the membrane was incubated with 1:2500 dilutions of appropriate secondary antibody for 2 hours at room temperature. The membrane was washed with PBST again, and Pierce ECL Western Blotting Substrate (Thermo Scientific) was used for development of immunoreactive bands. For immunoblotting of tissue samples, proteins were extracted in the same buffer with a tissue homogenizer after thawing frozen tissues collected by liquid nitrogen snap freezing.

Measurement of oxygen consumption rate and extracellular acidification rates

For Seahorse XFe96 assays, cells were seeded at pre-optimized final concentration 1.5×10^4 cells/well onto Seahorse XF-96-well plates and glycolysis stress and mito Stress tests were performed following the manufacturer's specifications (Seahorse Bioscience, North Billerica, MA). Each datum was determined minimally in triplicate. OCR and ECAR were reported as absolute rates (pmoles/min and OCR or mpH/min for ECAR) or normalized against cell counts, or expressed as a percentage of the baseline oxygen consumption

Cell Proliferation by FACS Analysis

A549 and A549 HK1b^{-/-} cells were trypsinized and harvested at 50%–70% confluency. Cells were fixed with ice-cold 70% ethanol dropwise while vortexing and incubated at minus 20 degree for a minimum of 24 hr. Fixed cells were pelleted and washed twice with PBS. *Anti-*

Human Ki-67, FITC kit is used to stain cells according to the manufacturers' protocol (BD Biosciences). Unstained and isotype-control stained cells are shown as controls. Cells were analyzed with a FACS AriaII flow cytometer and processed using FlowJo software

Annexin V assay

A549 and A549 HK1b^{-/-} cells were (2×10^5) treated with 75 μ M cisplatin and stained with Annexin V conjugated to Alexa Fluor 488 dye and propidium iodide (PI) using Dead Cell Apoptosis Kit (BD Biosciences) according to manufacturer's protocol. Briefly, the cells were harvested at 48 hours after treatment and suspended in Annexin V binding buffer at a concentration of 1×10^6 cells/mL. One-hundred microliters of cell suspension was incubated with 5 μ L of Annexin V and 1 μ L of 100 μ g/mL of PI for 15 minutes at room temperature. After the incubation period, the cells were analyzed FACS AriaII flow cytometer and processed using FlowJo software.

Sample Preparation for TEM

Cells were fixed with fixative mixture (0.08 M cacodylate pH 7.4, 2.5% paraformaldehyde, 1.25% glutaraldehyde and 2 mM calcium chloride) for 2 h at 4 °C washed and, were post-fixed in 2% OsO₄ aqueous solution for 20 min. Cells were incubated in 2.5% ferrocyanide for 20 min. Sequentially, the cells were incubated in 1% thiocarbonylhydrazide at 40 °C for 15 min, 2% OsO₄ for 20 min and 1% uranyl acetate at 4 °C for 30 min. Cells were warmed up to 50 °C for 30 min in uranyl acetate, washed twice in nanopure filtered water, were incubated in lead aspartate at 50 °C for 20 min. The samples were then dehydrated with graded alcohol series and then embedded in epoxy resin. After sectioning using an ultramicrotome (Leica EM UC7), samples were analyzed using an electron microscope (Carl Zeiss, Gemini 500).

DNA Fragmentation analysis

Standard Sensitivity NGS Fragment Analysis Kit (DNF-473-0500) is used for DNA fragmentation experiment and for dsDNA 905 Reagent Kit ((DNF-905-K0500) is used for visualization of 1-500bp PCR (Advanced Analytical Technologies, Inc., USA), according to manuscript protocol.

Structure Preparation:

We used crystal structures of HK1b (PDB ID: 1QHA) and HK2 (PDB ID: 2NZT), whereas HK1c was modeled using SWISS-Homology-Modeling-Software. Unresolved parts of the crystal structures were modeled with Swiss-Modeller, and loop regions were refined with ModLoop. The protonation states of residues were determined using PROPKA. Glucose was used in beta conformation. ATP and Mg²⁺ were translated to each system from crystal structure of Glucokinase (PDB ID: 3FGU).

Molecular Dynamics Simulations:

MD simulations were performed with GROMACS 5.1.4 employing CHARMM 36 force-field. Systems were subjected minimized using a conjugate gradient algorithm. All systems were

energy relaxed with 1000 steps of steepest-descent. The systems were equilibrated using NVT ensemble with Berendsen- algorithm. The final structures were run in NPT ensemble at 1 atm and 310 K. MD simulations were run for 300-ns. All coordinates were saved at 2-ps intervals for analysis. Long-range electrostatic forces were handled using PME, and Van der Waals forces treated with a 0.9-nm-cut-off. Water molecules were modelled with TIP3P model.

Expression and purification of recombinant human HK1b and HK1c isoforms.

The cloning service of recombinant human HK1b and HK1c isoforms was performed by GenScript Inc (Piscataway, NJ) using a pET28b bacterial expression vector. The expression and purification of human HK1 isoforms were performed as published previously in *E. coli* BL21-CodonPlus-RIL (Stratagene)⁴². The cell pellet was resuspended in lysis buffer (100 mM Tris, pH 7.4, 150 mM NaCl, 5 mM imidazole, 3 mM β ME, and protease inhibitor cocktail from Sigma-Aldrich: P8849), lysed by sonication, and centrifuged at 40,000xg for 45 min at 4 °C. The supernatants were loaded onto a Ni Sepharose 6 Fast Flow (GE Healthcare, Sweden) at 4 °C previously equilibrated with binding buffer (100 mM Tris, pH 7.4, 150 mM NaCl, 5 mM imidazole and 3 mM β ME). The columns were washed first with binding buffer then washing buffer (100 mM Tris, pH 7.4, 150 mM NaCl, 25 mM imidazole, 3 mM β ME). The HK1 isoforms were eluted with elution buffer supplemented with 300 mM imidazole. Finally, the proteins were loaded onto a HiLoad Superdex-S200 size-exclusion column (GE Healthcare) using AKTA purifier system (GE Healthcare). The gel filtration buffer contains 50 mM Hepes pH 7.4, 150 mM NaCl, and 0.5 mM TCEP. The protein peaks were collected and concentrated to 5 mg/mL, and the protein purity was assessed using SDS-PAGE.

CD spectroscopy and DSC measurements

The CD spectra of the HK1 isoforms were measured from 190 to 260 nm at 50 nm/min scanning speed and 0.5 nm bandwidth on a ChirascanTM CD spectrometer (Applied Photophysics). The enzyme concentration was 0.3 mg/mL in 50 mM phosphate buffer pH 7.4. The scans were measured at 25 °C using 1 mm quartz cuvette. Three scans were collected and averaged to reduce the noise of the CD scans. On the other hand, the thermodynamic stability of HK1 isoforms was determined in the absence and presence of 5 mM glucose using Nano-DSC (TA Instruments). The samples and buffers were degassed for 15 min with stirring at 10 °C. The DSC scans collected at protein concentration of 0.5 mg/mL in 50 mM Hepes pH 7.4 and 150 mM NaCl with a scan rate of 1° C/min from 10 to 80 °C at 3 atm pressure. Before loading the samples, background scans were obtained by loading degassed buffer (with or without glucose) in both reference and sample cells. The enthalpy of the transition (ΔH_{cal}) was estimated from the area under the thermal transition after subtracting the baseline by using Nano Analyzer software from TA instruments.

The enzymatic activity and initial velocity studies of HK1 isoforms

The HK1 reaction rate was determined by the G6P dehydrogenase (G6PDH) coupled spectrometric assay using Shimadzu UV-visible Spectrophotometer (UV-2700) equipped with CPS-100 temperature controller⁴². The reaction rate is determined by monitoring the amount of NADH produced by G6PDH at 340 nm ($\epsilon_{340nm} = 6220 \text{ M}^{-1} \text{ cm}^{-1}$) upon the oxidation of G6P. First, the reaction rate of HK1 isoforms was determined at different enzyme concentrations from 0.05 - 0.5 μM at fixed substrate concentrations of 3 mM ATP and 1 mM glucose in a reaction

buffer containing 50 mM HEPES pH 7.4, 150 mM NaCl, 20 mM MgCl₂, 3 mM NAD⁺, and 0.1 U/μL G6PDH. The data were fitted to a linear function using the Excel add-on package XL fit (IDBS limited, Bridgewater, NJ, U.S.A.) and the enzyme rate was calculated from the slope of the lines. On the other hand, the initial velocity studies of the HK1 isoforms were performed by measuring the enzymatic rate at different glucose 0.022 - 0.2 mM and ATP 0.24 - 1.2 mM concentrations. The double reciprocal plot of the data was used to determine the quality of the data that was fitted to a random sequential mechanism.

$$v = \frac{V_{max} AB}{K_a K_b + K_b A + K_a B + AB}$$

where v and V_{max} are initial and maximum velocities, respectively, A and B are substrate concentrations, and K_a and K_b are Michaelis constants for substrates A and B , respectively. Data were fitted using the Global fitting analysis in the kinetics module of SigmaPlot (Systat Software, Inc. San Jose, California, U.S.A).

Patient Tissue collection and immunohistochemical staining

This study was approved by the Ethics Committee of Istanbul Medipol University. 18 cases of clinically and immunohistologically verified frozen NSCLC primary tumor and normal lung tissue samples were collected from affiliated hospital of Istanbul Medipol University (Istanbul, Turkey) after getting patients' consent. All studies were conducted in accordance with the Declaration of Helsinki and guidelines on Good Clinical Practice. Immunostaining was performed on paraffin-embedded archival tissue at pathology department of Istanbul Medipol University hospital. In brief, the paraffin blocks were sliced into 4-μm thick sections, followed by deparaffinizing and rehydrating the section. After antigen retrieval, the sections were stained with indicated antibodies and staining of HK1 and Ki-67 was scored by pathologists based on the number of positive cells per area and staining intensity. Patients' clinical characteristics are listed in Table 1.

***In vivo* intra-tracheal and subcutaneous tumor xenograft tumorigenesis assay.**

NSG mice and nude mice (Nu-Nu) were purchased from The Jackson Laboratory and experiments were performed at the Istanbul Medipol University and Bilkent University, respectively. All mice were maintained in a specific pathogen-free facility in a temperature-regulated room (23±1°C) with a 12 h light/dark cycle. The protocols used were approved by the Institutional Animal Care and Use Committee of Istanbul Medipol University (Istanbul, Turkey) and Bilkent university (Ankara, Turkey). All animal experiments were performed in accordance with the provisions of the NIH Guide for the Care and Use of Laboratory 6-8 weeks old animals. 5x10⁶ x A549 WT and A549 HK1b^{-/-} cells were *intra-tracheally* injected into the right pleural cavity of NSG male mice. Approximately 3rd-4th intercostal space in the midclavicular line is used for injection. *Relative* tumor volume was measured 8 weeks after implantation and, is calculated as follows: (length × width × height) × π/6. End points were reached, and mice were killed once the tumor size measured 2000 mm³. For studies involving subcutaneous tumors generation, mice were injected with A549 WT and A549 HK1b^{-/-} cells (5 × 10⁶ cells in 100 μL of PBS) subcutaneously in the lower right flank of mice. Tumors were monitored for 48 days from the day of injection and *relative* tumor volume was calculated as follows: (length × width ×

height) $\times \pi/6$. Mice were sacrificed after 48 days, and tumor tissues were collected for further analyzing.

Patient Data Analyses

The publicly available Cancer Genome Atlas (TCGA) RNA-seq data on adenocarcinoma (n = 511) and SCC (n = 501) was used as an external cohort to verify DEGs between adenocarcinoma and SCC based on the RG cohort and to further analyze the expression of the HK1b isoform (transcript variant-8) between normal and TCGA Lung adenocarcinoma samples (RefSeq id NM_001322366). Lung Adenocarcinoma project contains 426 RNA sequencing of lung tumor tissues and matched with 602 normal lung tissues from the GTEx Project. For each database the supplied expected transcript read counts that are generated using the RSEM software package is used for the comparison. The read counts are normalized using the DESeq2 variance stabilized normalization method.

Gene expression data of lung cancers was extracted from the GEO database (accession number: [GSE31210](https://www.ncbi.nlm.nih.gov/geo/query/acc.cgi?acc=GSE31210), [GSE101929](https://www.ncbi.nlm.nih.gov/geo/query/acc.cgi?acc=GSE101929), [GSE10072](https://www.ncbi.nlm.nih.gov/geo/query/acc.cgi?acc=GSE10072) and [GSE32863](https://www.ncbi.nlm.nih.gov/geo/query/acc.cgi?acc=GSE32863)^{28, 39, 44, 61}). Calculation of HK1b knockout signature score was performed by subtracting the sum of z-scores of genes downregulated upon HK1b KO in A549 cells from the sum z-scores of the upregulated genes for each patient. Before GSEA, all lung cancer samples were divided into two groups according to their HK1 expression levels as HK1 high and HK1 low, or according to HK1b KO signature score levels as low HK1b KO score and high HK1 KO score. GSEA was then performed based on normalized data using GSEA v2.0 tool (<http://www.broad.mit.edu/gsea/>) for identification of enriched gene sets between two groups. Survival analysis was performed by separating patients based on median expression of HK1 ([GSE31210](https://www.ncbi.nlm.nih.gov/geo/query/acc.cgi?acc=GSE31210), and [GSE101929](https://www.ncbi.nlm.nih.gov/geo/query/acc.cgi?acc=GSE101929)) or 25th percentile (TCGA) of the HK1b KO signature score.

Statistical analysis.

Unless otherwise stated, data are expressed as mean \pm SEM. GraphPad Prism 8 and SPSS 18.0 software were used for graphing and statistical analysis. After calculating normality by Shapiro-Wilk test, Student *t* or Mann-Whitney test were used to compare two samples. For multiple group comparisons, One-way ANOVA analysis and followed by Tukey's multiple comparison tests were used. The significance for survival analyses was calculated using the Log-rank test in GraphPad Prism v8.0. Statistical parameters including exact value of n, statistical test and significance are reported in the figures and figure legends. Values of $p < 0.05$ were considered statistically significant.

FUNDING

This project was supported by European Molecular Biology Organization – EMBO [Installation Grant, grant number 6.8.3.778 to M.A.C.]

MAIN FIGURE LEGENDS

Figure 1. HK1 expression is upregulated in human NSCLC and is associated with a poor overall survival. (a and b) Protein was isolated from NSCLC tumor and adjacent-non tumor samples, HK1 and HK2 levels were determined by immunoblot analyses (a) Protein lysates of human NSCLC tumor (n=6), normal lung (n=4), (b) protein lysates of human NSCLC tumor (n=7), normal lung (n=6). (c) Quantification of HK1 and HK2 levels in NSCLC tumor (n = 13) and normal lung samples (n=10). (d) The prognostic value of HK1 in NSCLC patients from GSE31210 database (n=226). Tumors were separated into two groups according to HK1 expression levels (high or low). The high expression of HK1 is correlated to worse survival (p=0.011). (e) Immunohistochemical staining of HK1 expression and Hematoxylin&Eosin (H&E) staining in representative human NSCLC tumor (left) and the surrounding normal tissue (right). Images are 40X magnification; insets are 200X magnification. Scale bars, 100 μ m.

Figure 2. HK1b isoform levels were elevated in NSCLC tumors compared with normal lung tissue. (a and b) Representative semi q-PCR amplification results for HK1 isoforms, HK2 and p53 (a) in A549 WT cells, (b) in NSCLC patient tumors (n=3). (c) RNA was extracted from NSCLC patient normal lung and tumor samples, HK1b, HK1c and HK2 (normal n=6, tumor n=6) levels were determined by qRT-PCR. mRNA levels were normalized to ACTB mRNA. Data are from two or three independent experiment as triplicate, presented as mean \pm SEM, compared with Student's t test. (d) Kaplan–Meier plots showing the association of HK1b isoform overexpression between normal and TCGA Lung adenocarcinoma samples in patients from the TCGA cohort. (e and f) Kaplan–Meier survival curves for (e) adenocarcinoma (n=501) and (f) squamous cell carcinoma (n=489), patients stratified according to low or high HK1b expression levels. P values indicate significance levels from the comparison of survival curves using the Log-rank (Mantel-Cox) test.

Figure 3. Effect of HK1b knockout on metabolism and tumorigenicity of A549 cells. (a) A549–HK1b isoform-knockout cells were generated by using the CRISPR/ Cas9 genome editing system. A549 WT and A549 HK1b^{-/-} cells were analyzed by semi q-PCR and qRT-PCR for level of *HK1 a, b, c, HK2*. Error bars indicate mean \pm SEM, (n=3). (b) Representative immunofluorescence images after HK1b KO. Green, HK1; blue, DAPI. Scale bars, 20 μ m. (c) Immunoblot analysis of HK1b KO in A549 cells to determine the expression level of HK1. β -actin was used as a loading control. (d) A549 WT or A549 HK1b^{-/-} cells were *intra-tracheally* injected into immunodeficient NSG male mice. Graphs show tumor volume at endpoint at 8 weeks after A549 WT (control) or A549 HK1b^{-/-} injection (n=7, each). Tumor volumes presented as mean \pm SEM, compared with Student's t-test. (e) Mice were injected with A549 WT or A549 HK1b^{-/-} cells subcutaneously in the lower right flank of mice, and tumor volume was measured over a period of 56 days from the day of injection, *: p<0,05. (f) OCR values from Mitochondrial Stress Test performed with Seahorse XFe96 Analyzer. Oligomycin (2 μ M), FCCP (0,9 μ M) and Rotenone&Antimycin A (0,5 μ M) are inserted through *injection* ports *sequentially*. Experiments were performed at least twice in

quadruplicates. **(g)** Glycolysis Stress Test in A549 HK1b^{-/-} and A549 WT cells. Glucose (10 mM), Oligomycin (1 μ M) and 2-DG (50 mM) are injected sequentially. **(h)** Glycolysis stress test profile in A549 WT, A549 HK1b^{-/-} and A549 HK1b^{-/-}+HK1b cells and comparison of glycolysis levels. The results are presented as the mean \pm SEM and means compared with Student's t test, *: p<0,05. **(i)** Representative immunofluorescence images for A549 WT, A549 HK1b^{-/-} and HK1b fused A549 HK1b^{-/-} +HK1b) cells. Red, Mito Tracker; Green, HK1b EGFP; blue, DAPI. Scale bars, 10 μ m.

Figure 4. Loss of HK1b inhibits proliferation and demonstrates the clinical significance. **(a)** Ki-67 proliferation flow cytometry analysis of A549 WT and A549 HK1b^{-/-} cells. **(b)** HK1b KO signature scores of normal lungs vs. lung adenocarcinoma tissues from GSE10072 and GSE32863 human datasets. Data are represented as mean \pm standard deviation. **(c and d)** Gene set enrichment analysis in lung cancer patients from GSE101929 showing an enrichment of **(c)** glycolysis and **(d)** oxidative phosphorylation -related genes in patients expressing low HK1b KO signature score, i.e. those who have high HK1b levels. **(e)** Kaplan–Meier survival curve representing the percentage overall survival in lung adenocarcinoma cancer patients from TCGA (n = 255) separated based on low vs. high (25th percentile) HK1b KO signature score.

Figure 5. Biochemical, biophysical and computational characterization of human HK1b and HK1c. **(a)** RMSF Plot shows four major regions fluctuating in HK1c and HK-2 while HK1b is more stable. Structure of HK1c is shown in the figure, first region (1) responsible for ligand binding in N-terminal and a part of small sub-domain (which is responsible for opening and closing of ligands binding pocket), second region (2) ligand binding site in C-terminal part of small sub-domain, third region (3) C-terminal part of large domain and involved in ATP binding, fourth region (4) near to Glucose binding site of C-terminal large domain. **(b)** SDS-PAGE analysis and protein yield of HK1b and HK1c isoforms. The Coomassie-stain protein bands confirmed high purity >95% of the purified enzymes. The protein yield at the end of purification was 6.8 and 2.2 mg of protein per liter of E. coli culture for HK1b and HK1c isoforms, respectively. **(c)** Far-UV CD spectra of HK1b (black) and HK1c (red) isoforms in the absence of substrates with minima at 208 and 222 nm. The CD spectra is a good representation of a natively α/β folded protein. **(d)** DSC thermograms in the absence (solid line) and presence (dashed line) of 5 mM glucose. DSC scans were corrected for buffer base line and data fitted to one-state transition for HK1b (black) or two-state transitions for HK1c (red). Data are mean \pm S.D., n=3. **(e)** The enzymatic rate and relative enzyme activity (%). The rate of HK1b (black) and HK1c (red) reaction was measured at different enzyme concentrations and substrates were fixed at saturated concentrations of 1 mM glucose and 3 mM ATP. The relative enzyme activity was determined from the slope of the lines. **(f)** The double-reciprocal plots of initial rate as a function of glucose and ATP for HK1b and HK1c isoforms. The rates were obtained by varying glucose at different fixed concentrations of ATP. The points represent experimental data and lines are theoretical fit of the data that are expressed as mean with standard deviation (n = 3).

Figure 6. Effect of HK1b depletion and cisplatin on A549 cells. (a) A549 WT and A549 HK1b^{-/-} cells were treated with increasing concentrations of Cisplatin (0 μ M–200 μ M) for 48 hrs. Dose-response curves were generated from which IC50 values were deduced (n=3). (b) Quantification of apoptosis by Flow cytometry analysis of Annexin V-FITC and PI propidium iodide (PI) staining in A549 WT and A549 HK1b^{-/-} cells. (c, d and e) Immunoblot analyses of cell lysates with Cisplatin (75 μ M-48 hours) treatment were done to determine the levels of (c) cleaved PARP, cleaved Caspase-3, Bcl-2, (d) BAX, (e) P-p53, total p53, P-GSK3 β , total GSK3 β , P-ERK and total ERK. Anti- β -actin is used as a loading control. (f) Band densities of p53 and phospho-p53 were measured using Image J software. Quantified blots were normalized to β -actin and are expressed as -fold increase relative to the untreated A549 WT. Error bars indicate the mean \pm S.E.M. (n = 3). Statistical significance assessed by One-way ANOVA and Bonferroni's multiple comparisons test. (g) A549 WT, A549 HK1b^{-/-} and A549 HK1b^{-/-} +HK1b cells were treated with increasing concentrations of Cisplatin (0 μ M–200 μ M) for 48 h. Dose-response curves were generated from which IC50 values were deduced (n=3). (h) Representative semi q-PCR amplification results for HK1b in A549 WT, A549 HK1b^{-/-} and A549 HK1b^{-/-} +HK1b cells.

Figure 7. Synergetic effects of HK1b ablation and cisplatin on apoptotic and autophagic cell death. (a) Immunoblot analysis of LC3B I/II, P-mTOR and P-H2AX in Cisplatin (75 μ M-48 hours) treated A549 WT and A549 HK1b^{-/-} cells. Anti- β -actin is used as a loading control. (b) Band densities of phospho-H2AX were measured using Image J software. Quantified blots were normalized to β -actin and are expressed as -fold increase relative to the untreated A549 WT. Error bars indicate the mean \pm S.E.M. (n = 3). Statistical significance assessed by One-way ANOVA and Bonferroni's multiple comparisons test. (c and d) Gene set enrichment analysis in lung cancer patients from GSE101929 showing an enrichment of (c) autophagy and (d) DNA repair -related genes in patients expressing low HK1b KO signature score, i.e. those who have high HK1b levels. (e) Representative Transmission Electron Microscopy (TEM) micrographs displaying characteristics of autophagy; images are representative of two independent experiments; scale bar, 2 μ m (left) and 400 \square nm (right). '*': myelinoid bodies; red arrows: autophagic vesicle.

SUPPLEMENTARY FIGURE LEGENDS:

Fig. S1: Schematic representation of three HK1 isoforms (*HK1a, b, and c*) and model of *HK1 b* and *c* structural differences. (a) RefSeq gene annotations of HK1 isoforms (HK1a, HK1b and HK1c) and HK2. HK1a and HK1b isoforms possess one extra exon, exon 8, which is missing in HK1c. (b) Structural alignment between crystal structures of HK1b and HK1c model. The extra exon in HK1b, which is shown in blue, codes for 32-amino acid long alpha-helix that is part of the small sub-domain of N-terminus. For the sake of simplicity only one monomer is shown.

Fig. S2: Analysis of isogenic clones expressing sgHK1b. (a) PCR and DNA fragmentation analysis of HK1b isoform elimination at the target loci, indicating deletion of 14 bp nucleotides resulting in a frame-shift mutation. (b) A549 WT, A549 HK1b^{-/-}, and as a control H1299 cells were analyzed by semi q-PCR for level of HK1 a, b, c, HK2, and p53.

Fig. S3: Histopathological evaluation of A549 WT or A549 HK1b^{-/-} tumors in both intra-tracheal and subcutaneous xenograft models.

(a and c) Immunohistochemical staining of HK1 expression and H&E staining in representative mouse (a) intra-tracheal xenograft models of lung cancer (c) subcutaneous xenograft models of lung cancer- in both A549WT tumor (left) and A549 HK1b^{-/-} tumor (right). Images are 40X magnification; insets are 200X magnification. Scale bars, 100 μ m. (b and d) Representative photographs of Ki-67 expression in (b) intra-tracheal (d) subcutaneous - xenografts of A549 WT (left) and A549 HK1b^{-/-} (right) stained by IHC in upper panel. Number of Ki-67 positive cells is counted per area (mm²) from 5 different fields in 8 different slides. The results are presented as the mean \pm SEM and means compared with Student's t test.

Fig. S4: Effect of HK1b depletion combined with cisplatin of A549 cells in time-response evaluation. (a) Immunoblot analyses of cell lysates with Cisplatin (75 μ M) treatment at 12hrs and 24hrs, respectively were done to determine the levels of cleaved PARP, cleaved Caspase-3; Bcl-2 and Anti- β -actin. (b) Immunoblot analyses of cell lysates with Cisplatin (75 μ M) treatment at 12hrs was done to determine the levels of P-p53, total p53, P-GSK3 β , total GSK3 β , P-ERK and total ERK. (c) Immunoblot analyses of cell lysates with Cisplatin (75 μ M) treatment at 12hrs was done to determine the levels of P-H2AX. (d) Band densities of phospho-H2AX were measured using Image J software. Quantified blots were normalized to β -actin and are expressed as -fold increase relative to the untreated A549 WT. Error bars indicate the mean \pm S.E.M. (n = 3). Statistical significance assessed by One-way ANOVA and Bonferroni's multiple comparisons test.

Supplementary Table 1: List of total 18 NSCLC patients' clinical details is included in this study.

REFERENCES:

- 1 Ali A, Goffin JR, Arnold A, Ellis PM. Survival of patients with non-small-cell lung cancer after a diagnosis of brain metastases. *Current oncology (Toronto, Ont)* 2013; 20: e300-306.
- 2 Arzoine L, Zilberberg N, Ben-Romano R, Shoshan-Barmatz V. Voltage-dependent anion channel 1-based peptides interact with hexokinase to prevent its anti-apoptotic activity. *The Journal of biological chemistry* 2009; 284: 3946-3955.
- 3 Bao L, Jaramillo MC, Zhang Z, Zheng Y, Yao M, Zhang DD *et al*. Induction of autophagy contributes to cisplatin resistance in human ovarian cancer cells. *Molecular medicine reports* 2015; 11: 91-98.
- 4 Bhatt AN, Chauhan A, Khanna S, Rai Y, Singh S, Soni R *et al*. Transient elevation of glycolysis confers radio-resistance by facilitating DNA repair in cells. *BMC cancer* 2015; 15: 335.
- 5 Bray NL, Pimentel H, Melsted P, Pachter L. Near-optimal probabilistic RNA-seq quantification. *Nature biotechnology* 2016; 34: 525-527.
- 6 Capello M, Ferri-Borgogno S, Riganti C, Chattaragada MS, Principe M, Roux C *et al*. Targeting the Warburg effect in cancer cells through ENO1 knockdown rescues oxidative phosphorylation and induces growth arrest. *Oncotarget* 2016; 7: 5598-5612.
- 7 Caunt CJ, Sale MJ, Smith PD, Cook SJ. MEK1 and MEK2 inhibitors and cancer therapy: the long and winding road. *Nature reviews Cancer* 2015; 15: 577-592.
- 8 Cesar Mde C, Wilson JE. Further studies on the coupling of mitochondrially bound hexokinase to intramitochondrially compartmented ATP, generated by oxidative phosphorylation. *Archives of biochemistry and biophysics* 1998; 350: 109-117.
- 9 Christofk HR, Vander Heiden MG, Harris MH, Ramanathan A, Gerszten RE, Wei R *et al*. The M2 splice isoform of pyruvate kinase is important for cancer metabolism and tumour growth. *Nature* 2008; 452: 230-233.
- 10 Chu Y, Chang Y, Lu W, Sheng X, Wang S, Xu H *et al*. Regulation of Autophagy by Glycolysis in Cancer. *Cancer management and research* 2020; 12: 13259-13271.
- 11 Dasari S, Tchounwou PB. Cisplatin in cancer therapy: molecular mechanisms of action. *European journal of pharmacology* 2014; 740: 364-378.
- 12 Desilet N, Campbell TN, Choy FY. p53-based anti-cancer therapies: An empty promise? *Current issues in molecular biology* 2010; 12: 143-146.

- 13 Ding Q, Xia W, Liu JC, Yang JY, Lee DF, Xia J *et al.* Erk associates with and primes GSK-3beta for its inactivation resulting in upregulation of beta-catenin. *Molecular cell* 2005; 19: 159-170.
- 14 Doherty J, Baehrecke EH. Life, death and autophagy. *Nature cell biology* 2018; 20: 1110-1117.
- 15 Eliopoulos AG, Havaki S, Gorgoulis VG. DNA Damage Response and Autophagy: A Meaningful Partnership. *Frontiers in genetics* 2016; 7: 204.
- 16 Frame S, Cohen P. GSK3 takes centre stage more than 20 years after its discovery. *The Biochemical journal* 2001; 359: 1-16.
- 17 Gelb BD, Adams V, Jones SN, Griffin LD, MacGregor GR, McCabe ER. Targeting of hexokinase 1 to liver and hepatoma mitochondria. *Proceedings of the National Academy of Sciences of the United States of America* 1992; 89: 202-206.
- 18 Goodwin J, Neugent ML, Lee SY, Choe JH, Choi H, Jenkins DMR *et al.* The distinct metabolic phenotype of lung squamous cell carcinoma defines selective vulnerability to glycolytic inhibition. *Nature communications* 2017; 8: 15503.
- 19 Gottlob K, Majewski N, Kennedy S, Kandel E, Robey RB, Hay N. Inhibition of early apoptotic events by Akt/PKB is dependent on the first committed step of glycolysis and mitochondrial hexokinase. *Genes & development* 2001; 15: 1406-1418.
- 20 Govoni M, Rossi V, Di Stefano G, Manerba M. Lactate Upregulates the Expression of DNA Repair Genes, Causing Intrinsic Resistance of Cancer Cells to Cisplatin. *Pathology oncology research : POR* 2021; 27: 1609951.
- 21 Hanahan D, Weinberg RA. Hallmarks of cancer: the next generation. *Cell* 2011; 144: 646-674.
- 22 He X, Lin X, Cai M, Zheng X, Lian L, Fan D *et al.* Overexpression of Hexokinase 1 as a poor prognosticator in human colorectal cancer. *Tumour biology : the journal of the International Society for Oncodevelopmental Biology and Medicine* 2016; 37: 3887-3895.
- 23 Hong DS, Fakih MG, Strickler JH, Desai J, Durm GA, Shapiro GI *et al.* KRAS(G12C) Inhibition with Sotorasib in Advanced Solid Tumors. *The New England journal of medicine* 2020; 383: 1207-1217.
- 24 Hooft L, van der Veldt AA, van Diest PJ, Hoekstra OS, Berkhof J, Teule GJ *et al.* [18F]fluorodeoxyglucose uptake in recurrent thyroid cancer is related to hexokinase i expression in the primary tumor. *The Journal of clinical endocrinology and metabolism* 2005; 90: 328-334.

- 25 Jiao L, Zhang HL, Li DD, Yang KL, Tang J, Li X *et al*. Regulation of glycolytic metabolism by autophagy in liver cancer involves selective autophagic degradation of HK2 (hexokinase 2). *Autophagy* 2018; 14: 671-684.
- 26 John S, Weiss JN, Ribalet B. Subcellular localization of hexokinases I and II directs the metabolic fate of glucose. *PloS one* 2011; 6: e17674.
- 27 Kang C, Xu Q, Martin TD, Li MZ, Demaria M, Aron L *et al*. The DNA damage response induces inflammation and senescence by inhibiting autophagy of GATA4. *Science (New York, NY)* 2015; 349: aaa5612.
- 28 Landi MT, Dracheva T, Rotunno M, Figueroa JD, Liu H, Dasgupta A *et al*. Gene expression signature of cigarette smoking and its role in lung adenocarcinoma development and survival. *PloS one* 2008; 3: e1651.
- 29 Lin X, Xiao Z, Chen T, Liang SH, Guo H. Glucose Metabolism on Tumor Plasticity, Diagnosis, and Treatment. *Frontiers in oncology* 2020; 10: 317.
- 30 Linardou H, Dahabreh IJ, Kanaloupiti D, Siannis F, Bafaloukos D, Kosmidis P *et al*. Assessment of somatic k-RAS mutations as a mechanism associated with resistance to EGFR-targeted agents: a systematic review and meta-analysis of studies in advanced non-small-cell lung cancer and metastatic colorectal cancer. *The Lancet Oncology* 2008; 9: 962-972.
- 31 Liu PP, Liao J, Tang ZJ, Wu WJ, Yang J, Zeng ZL *et al*. Metabolic regulation of cancer cell side population by glucose through activation of the Akt pathway. *Cell death and differentiation* 2014; 21: 124-135.
- 32 Lu KT, Kanno Y, Cannons JL, Handon R, Bible P, Elkahloun AG *et al*. Functional and epigenetic studies reveal multistep differentiation and plasticity of in vitro-generated and in vivo-derived follicular T helper cells. *Immunity* 2011; 35: 622-632.
- 33 Luengo A, Gui DY, Vander Heiden MG. Targeting Metabolism for Cancer Therapy. *Cell chemical biology* 2017; 24: 1161-1180.
- 34 Majewski N, Nogueira V, Bhaskar P, Coy PE, Skeen JE, Gottlob K *et al*. Hexokinase-mitochondria interaction mediated by Akt is required to inhibit apoptosis in the presence or absence of Bax and Bak. *Molecular cell* 2004; 16: 819-830.
- 35 Marko AJ, Miller RA, Kelman A, Frauwirth KA. Induction of glucose metabolism in stimulated T lymphocytes is regulated by mitogen-activated protein kinase signaling. *PloS one* 2010; 5: e15425.
- 36 Mathew R, Karantza-Wadsworth V, White E. Role of autophagy in cancer. *Nature reviews Cancer* 2007; 7: 961-967.

- 37 Mathupala SP, Ko YH, Pedersen PL. Hexokinase II: cancer's double-edged sword acting as both facilitator and gatekeeper of malignancy when bound to mitochondria. *Oncogene* 2006; 25: 4777-4786.
- 38 Min J, Huang K, Tang H, Ding X, Qi C, Qin X *et al.* Phloretin induces apoptosis of non-small cell lung carcinoma A549 cells via JNK1/2 and p38 MAPK pathways. *Oncology reports* 2015; 34: 2871-2879.
- 39 Mitchell KA, Zingone A, Toulabi L, Boeckelman J, Ryan BM. Comparative transcriptome profiling reveals coding and noncoding RNA differences in NSCLC from African Americans and European Americans. *Clinical Cancer Research* 2017; 23: 7412-7425.
- 40 Mori C, Welch JE, Fulcher KD, O'Brien DA, Eddy EM. Unique hexokinase messenger ribonucleic acids lacking the porin-binding domain are developmentally expressed in mouse spermatogenic cells. *Biology of reproduction* 1993; 49: 191-203.
- 41 Mori C, Nakamura N, Welch JE, Shiota K, Eddy EM. Testis-specific expression of mRNAs for a unique human type 1 hexokinase lacking the porin-binding domain. *Molecular reproduction and development* 1996; 44: 14-22.
- 42 Nawaz MH, Ferreira JC, Nedyalkova L, Zhu H, Carrasco-López C, Kirmizialtin S *et al.* The catalytic inactivation of the N-half of human hexokinase 2 and structural and biochemical characterization of its mitochondrial conformation. *Bioscience reports* 2018; 38.
- 43 Ohba S, Johannessen TA, Chatla K, Yang X, Pieper RO, Mukherjee J. Phosphoglycerate Mutase 1 Activates DNA Damage Repair via Regulation of WIP1 Activity. *Cell reports* 2020; 31: 107518.
- 44 Okayama H, Kohno T, Ishii Y, Shimada Y, Shiraishi K, Iwakawa R *et al.* Identification of genes upregulated in ALK-positive and EGFR/KRAS/ALK-negative lung adenocarcinomas. *Cancer research* 2012; 72: 100-111.
- 45 Olausson KA, Dunant A, Fouret P, Brambilla E, Andre F, Haddad V *et al.* DNA repair by ERCC1 in non-small-cell lung cancer and cisplatin-based adjuvant chemotherapy. *The New England journal of medicine* 2006; 355: 983-991.
- 46 Oparina NY, Snezhkina AV, Sadritdinova AF, Veselovskii VA, Dmitriev AA, Senchenko VN *et al.* [Differential expression of genes that encode glycolysis enzymes in kidney and lung cancer in humans]. *Genetika* 2013; 49: 814-823.
- 47 Papa S, Choy PM, Bubici C. The ERK and JNK pathways in the regulation of metabolic reprogramming. *Oncogene* 2019; 38: 2223-2240.

- 48 Pastorino JG, Hoek JB, Shulga N. Activation of glycogen synthase kinase 3beta disrupts the binding of hexokinase II to mitochondria by phosphorylating voltage-dependent anion channel and potentiates chemotherapy-induced cytotoxicity. *Cancer research* 2005; 65: 10545-10554.
- 49 Pastorino JG, Hoek JB. Regulation of hexokinase binding to VDAC. *Journal of bioenergetics and biomembranes* 2008; 40: 171-182.
- 50 Persons DL, Yazlovitskaya EM, Pelling JC. Effect of extracellular signal-regulated kinase on p53 accumulation in response to cisplatin. *The Journal of biological chemistry* 2000; 275: 35778-35785.
- 51 Porporato PE, Filigheddu N, Pedro JMB, Kroemer G, Galluzzi L. Mitochondrial metabolism and cancer. *Cell research* 2018; 28: 265-280.
- 52 Qian X, Xu W, Xu J, Shi Q, Li J, Weng Y *et al.* Enolase 1 stimulates glycolysis to promote chemoresistance in gastric cancer. *Oncotarget* 2017; 8: 47691-47708.
- 53 Ran FA, Hsu PD, Wright J, Agarwala V, Scott DA, Zhang F. Genome engineering using the CRISPR-Cas9 system. *Nature protocols* 2013; 8: 2281-2308.
- 54 Rasola A, Sciacovelli M, Chiara F, Pantic B, Brusilow WS, Bernardi P. Activation of mitochondrial ERK protects cancer cells from death through inhibition of the permeability transition. *Proceedings of the National Academy of Sciences of the United States of America* 2010; 107: 726-731.
- 55 Roberts DJ, Tan-Sah VP, Smith JM, Miyamoto S. Akt phosphorylates HK-II at Thr-473 and increases mitochondrial HK-II association to protect cardiomyocytes. *The Journal of biological chemistry* 2013; 288: 23798-23806.
- 56 Roberts DJ, Tan-Sah VP, Ding EY, Smith JM, Miyamoto S. Hexokinase-II positively regulates glucose starvation-induced autophagy through TORC1 inhibition. *Molecular cell* 2014; 53: 521-533.
- 57 Robey RB, Hay N. Mitochondrial hexokinases, novel mediators of the antiapoptotic effects of growth factors and Akt. *Oncogene* 2006; 25: 4683-4696.
- 58 Rosano C. Molecular model of hexokinase binding to the outer mitochondrial membrane porin (VDAC1): Implication for the design of new cancer therapies. *Mitochondrion* 2011; 11: 513-519.
- 59 Rose IA, Warms JV. Mitochondrial hexokinase. Release, rebinding, and location. *The Journal of biological chemistry* 1967; 242: 1635-1645.
- 60 Schindler A, Foley E. Hexokinase 1 blocks apoptotic signals at the mitochondria. *Cellular signalling* 2013; 25: 2685-2692.

- 61 Selamat SA, Chung BS, Girard L, Zhang W, Zhang Y, Campan M *et al.* Genome-scale analysis of DNA methylation in lung adenocarcinoma and integration with mRNA expression. *Genome research* 2012; 22: 1197-1211.
- 62 Shi S, Tan P, Yan B, Gao R, Zhao J, Wang J *et al.* ER stress and autophagy are involved in the apoptosis induced by cisplatin in human lung cancer cells. *Oncology reports* 2016; 35: 2606-2614.
- 63 Sidaway P. Sotorasib effective in KRAS-mutant NSCLC. *Nature reviews Clinical oncology* 2021; 18: 470.
- 64 Sobanski T, Rose M, Suraweera A, O'Byrne K, Richard DJ, Bolderson E. Cell Metabolism and DNA Repair Pathways: Implications for Cancer Therapy. *Frontiers in cell and developmental biology* 2021; 9: 633305.
- 65 Stephen AG, Esposito D, Bagni RK, McCormick F. Dragging ras back in the ring. *Cancer cell* 2014; 25: 272-281.
- 66 Tang D, Wu D, Hirao A, Lahti JM, Liu L, Mazza B *et al.* ERK activation mediates cell cycle arrest and apoptosis after DNA damage independently of p53. *The Journal of biological chemistry* 2002; 277: 12710-12717.
- 67 Tiscornia G, Singer O, Verma IM. Production and purification of lentiviral vectors. *Nature protocols* 2006; 1: 241-245.
- 68 Trenner A, Sartori AA. Harnessing DNA Double-Strand Break Repair for Cancer Treatment. *Frontiers in oncology* 2019; 9: 1388.
- 69 van Vugt MA. Shutting down the power supply for DNA repair in cancer cells. *The Journal of cell biology* 2017; 216: 295-297.
- 70 Vander Heiden MG, Cantley LC, Thompson CB. Understanding the Warburg effect: the metabolic requirements of cell proliferation. *Science (New York, NY)* 2009; 324: 1029-1033.
- 71 Vanzo R, Bartkova J, Merchut-Maya JM, Hall A, Bouchal J, Dyrskjøt L *et al.* Autophagy role(s) in response to oncogenes and DNA replication stress. *Cell death and differentiation* 2020; 27: 1134-1153.
- 72 Varghese E, Samuel SM, Líšková A, Samec M, Kubatka P, Büsselberg D. Targeting Glucose Metabolism to Overcome Resistance to Anticancer Chemotherapy in Breast Cancer. *Cancers* 2020; 12.

- 73 Wang H, Wang L, Zhang Y, Wang J, Deng Y, Lin D. Erratum to: Inhibition of glycolytic enzyme hexokinase II (HK2) suppresses lung tumor growth. *Cancer cell international* 2016; 16: 38.
- 74 Wang J, Wu GS. Role of autophagy in cisplatin resistance in ovarian cancer cells. *The Journal of biological chemistry* 2014; 289: 17163-17173.
- 75 Wang X, Martindale JL, Holbrook NJ. Requirement for ERK activation in cisplatin-induced apoptosis. *The Journal of biological chemistry* 2000; 275: 39435-39443.
- 76 Waskova-Arnostova P, Elsnicova B, Kasparova D, Sebesta O, Novotny J, Neckar J *et al.* Right-to-left ventricular differences in the expression of mitochondrial hexokinase and phosphorylation of Akt. *Cellular physiology and biochemistry : international journal of experimental cellular physiology, biochemistry, and pharmacology* 2013; 31: 66-79.
- 77 Weng HC, Sung CJ, Hsu JL, Leu WJ, Guh JH, Kung FL *et al.* The Combination of a Novel GLUT1 Inhibitor and Cisplatin Synergistically Inhibits Breast Cancer Cell Growth By Enhancing the DNA Damaging Effect and Modulating the Akt/mTOR and MAPK Signaling Pathways. *Frontiers in pharmacology* 2022; 13: 879748.
- 78 Wilson JE. Isozymes of mammalian hexokinase: structure, subcellular localization and metabolic function. *The Journal of experimental biology* 2003; 206: 2049-2057.
- 79 Xu S, Herschman HR. A Tumor Agnostic Therapeutic Strategy for Hexokinase 1-Null/Hexokinase 2-Positive Cancers. *Cancer research* 2019; 79: 5907-5914.
- 80 Yang W, Zheng Y, Xia Y, Ji H, Chen X, Guo F *et al.* ERK1/2-dependent phosphorylation and nuclear translocation of PKM2 promotes the Warburg effect. *Nature cell biology* 2012; 14: 1295-1304.
- 81 Zerbino DR, Achuthan P, Akanni W, Amode MR, Barrell D, Bhai J *et al.* Ensembl 2018. *Nucleic acids research* 2018; 46: D754-d761.
- 82 Zhang XY, Zhang M, Cong Q, Zhang MX, Zhang MY, Lu YY *et al.* Hexokinase 2 confers resistance to cisplatin in ovarian cancer cells by enhancing cisplatin-induced autophagy. *The international journal of biochemistry & cell biology* 2018; 95: 9-16.

Figure 1

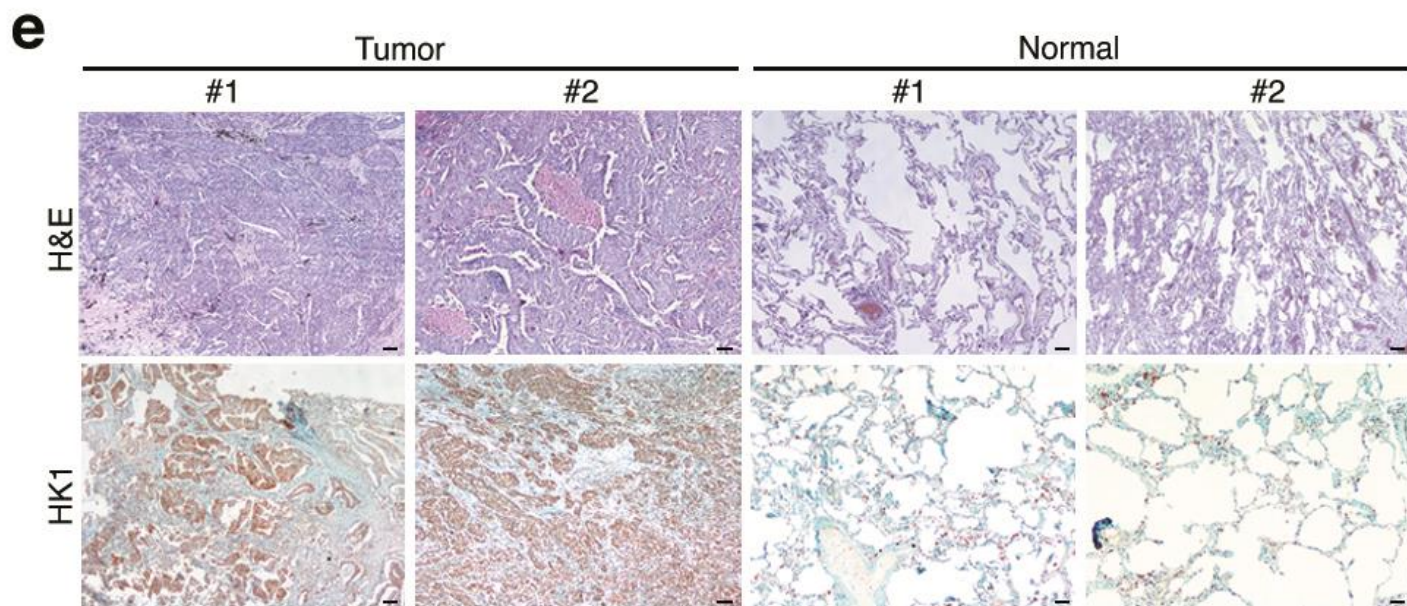
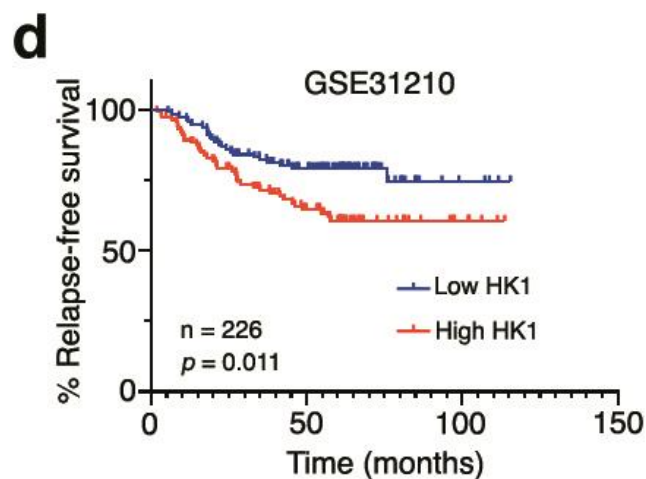
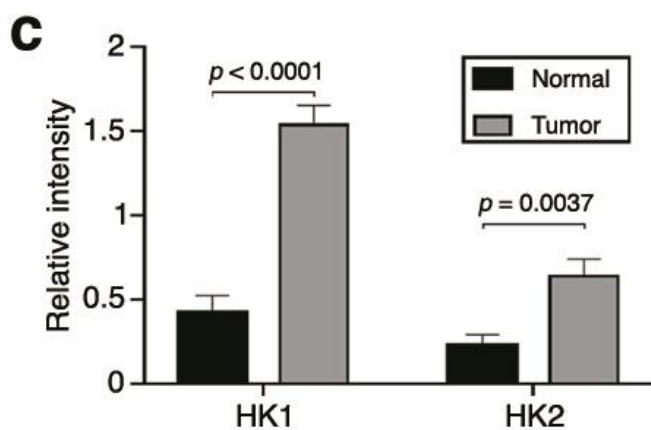
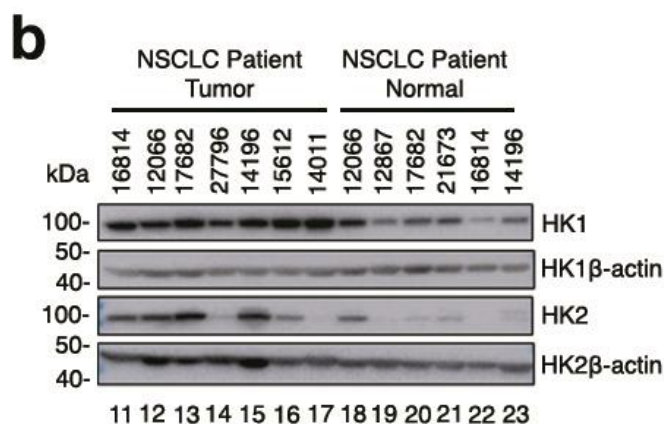
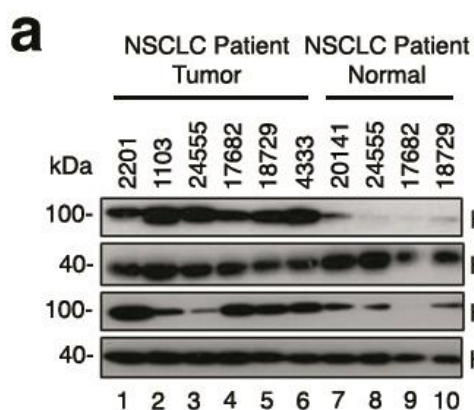


Figure 2

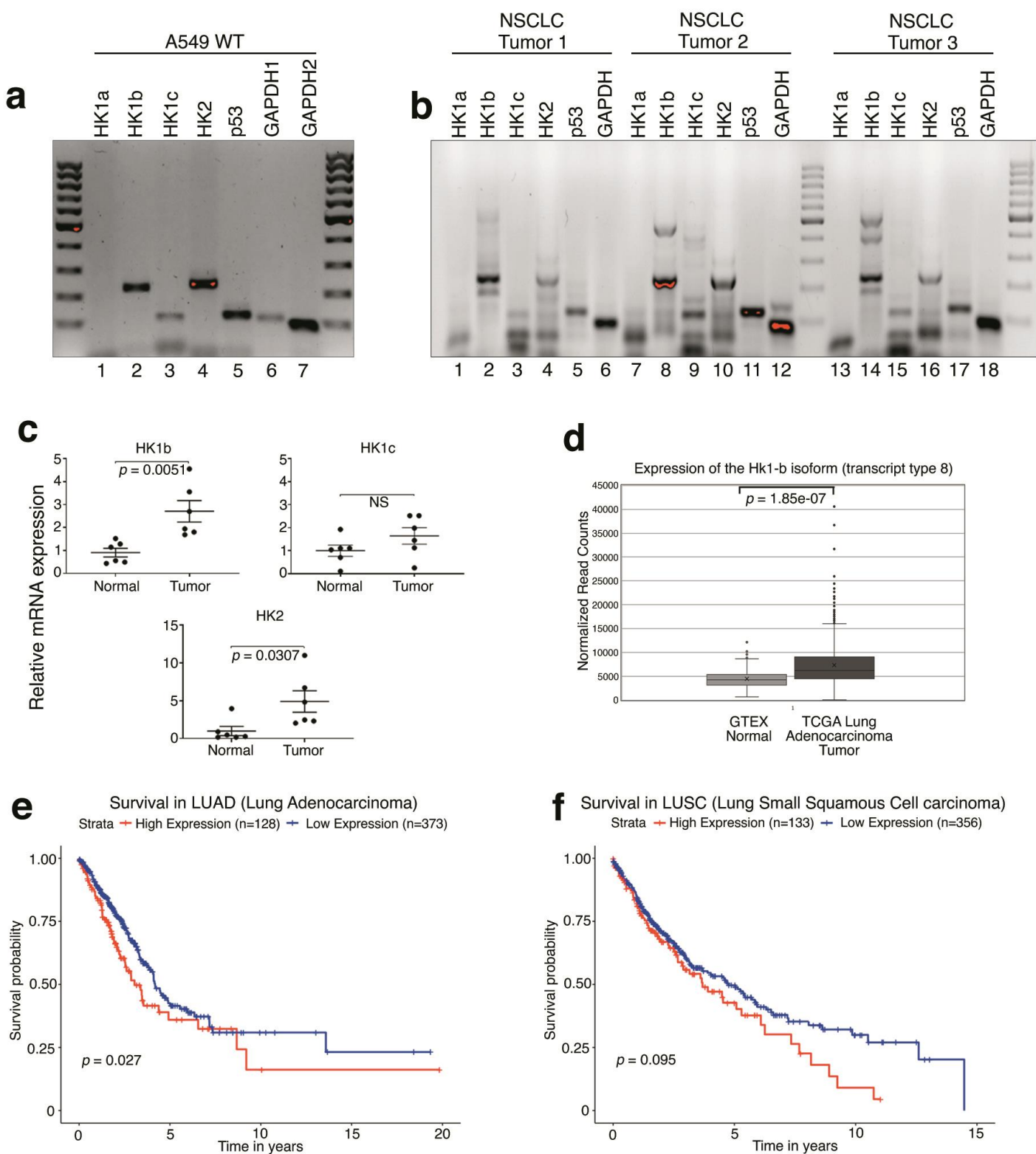


Figure 3

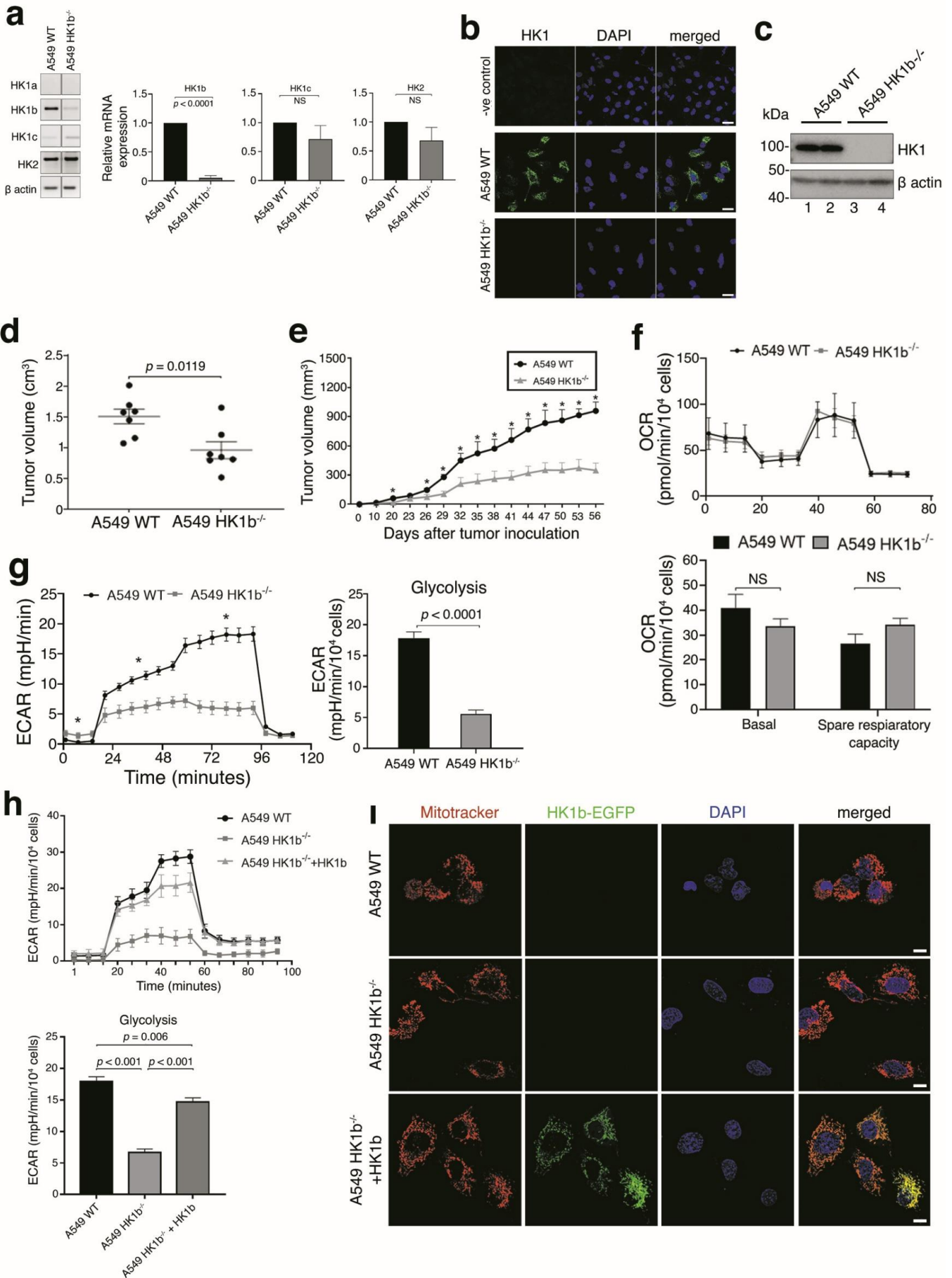


Figure 4

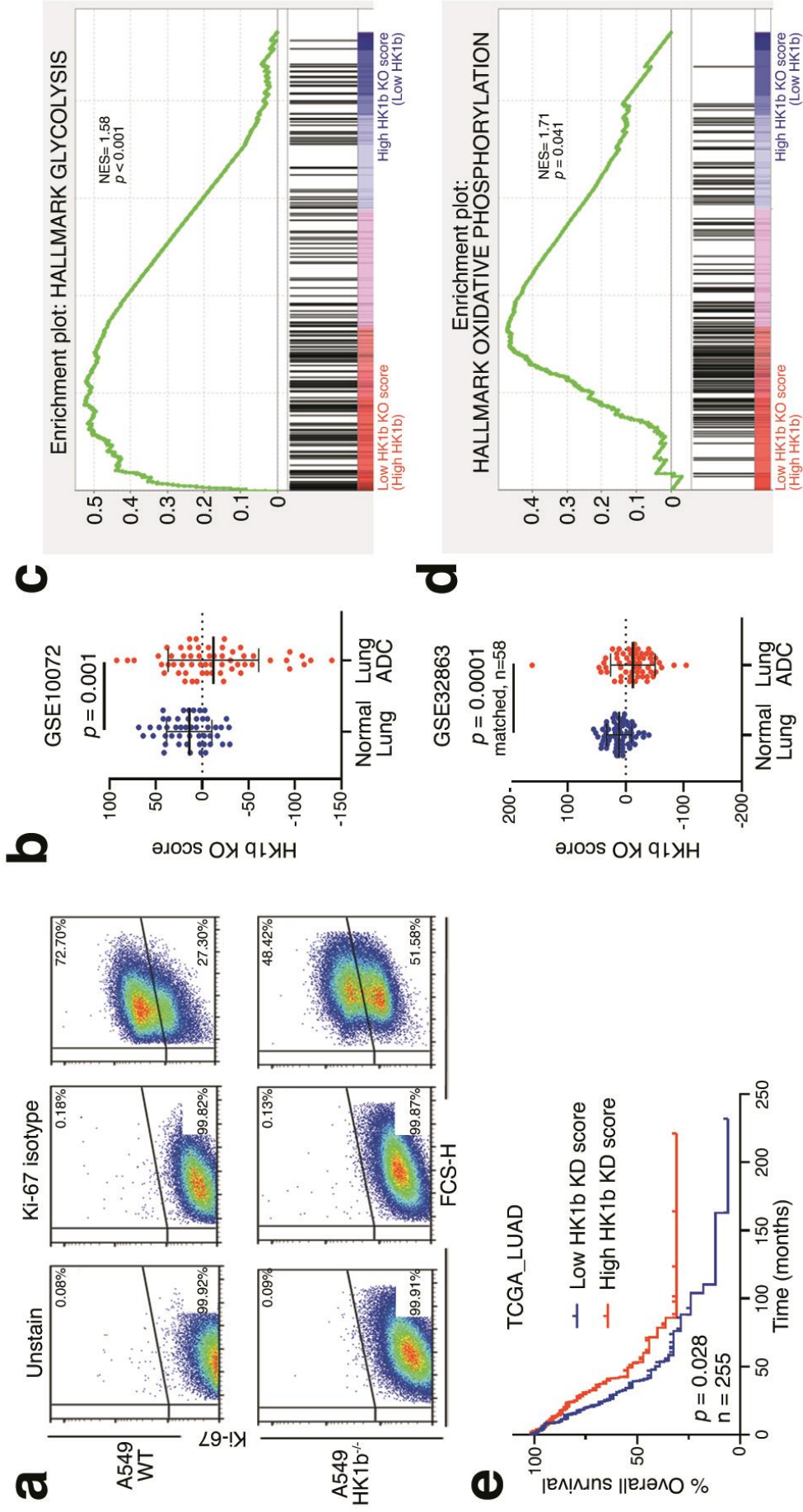


Figure 5

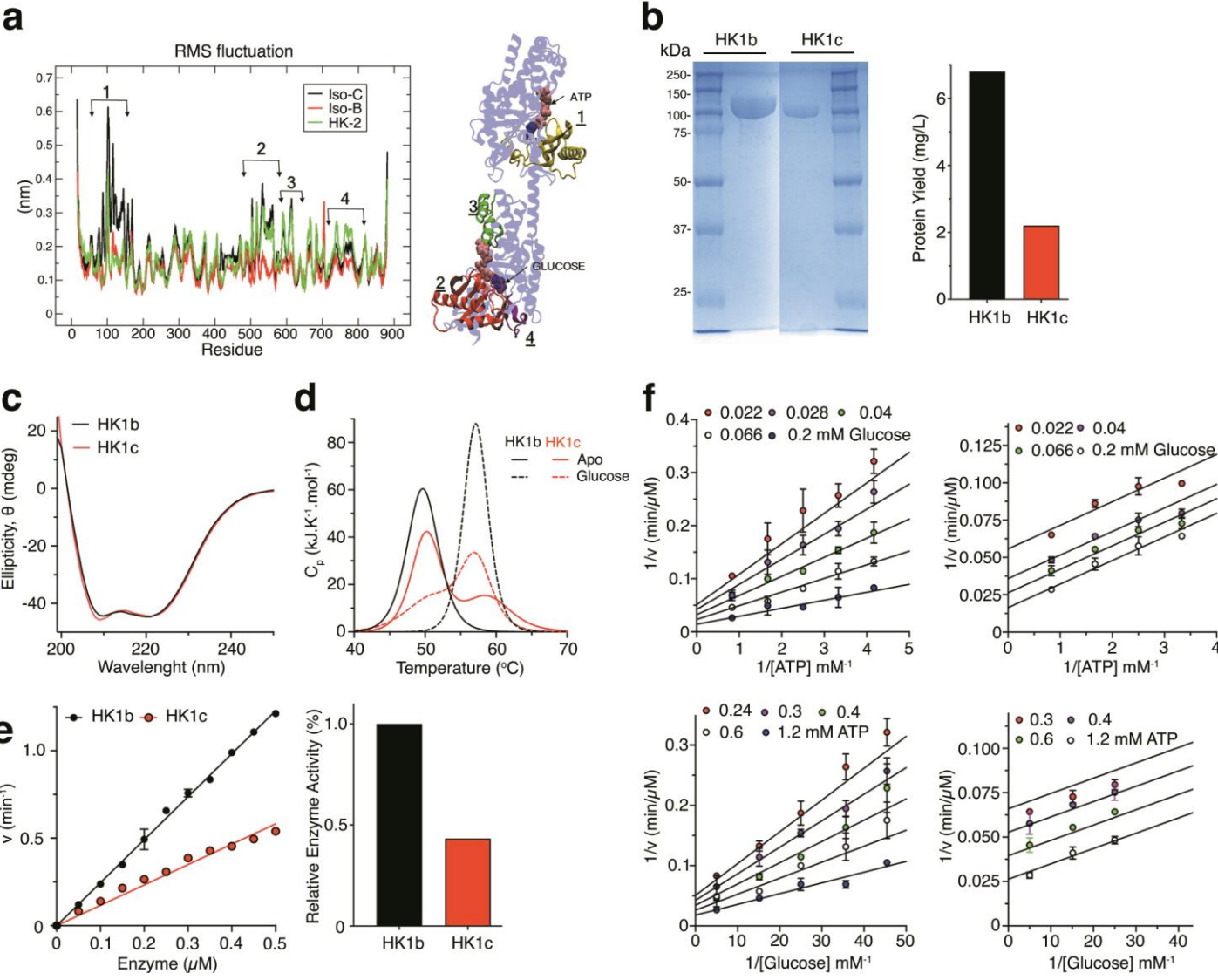


Figure 6

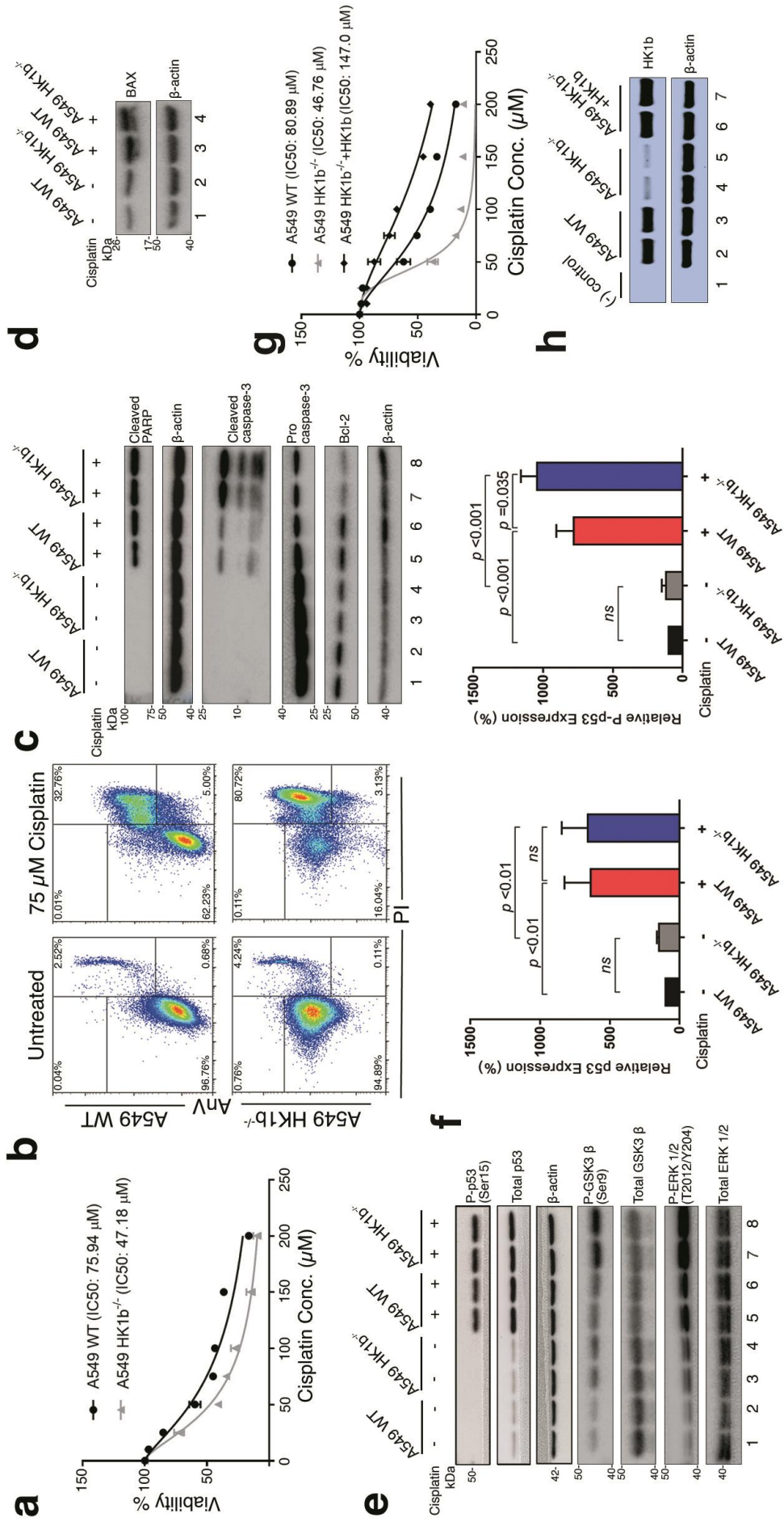
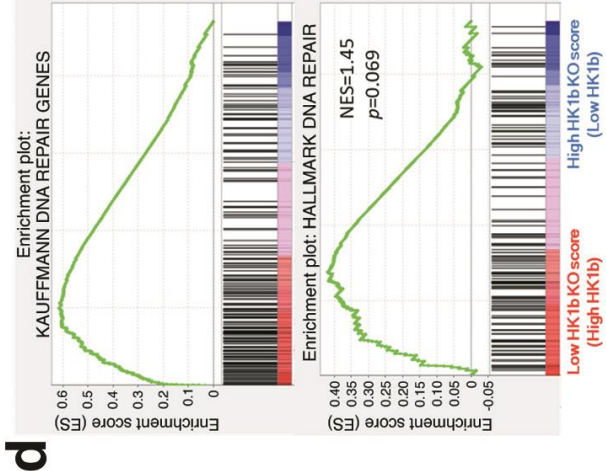
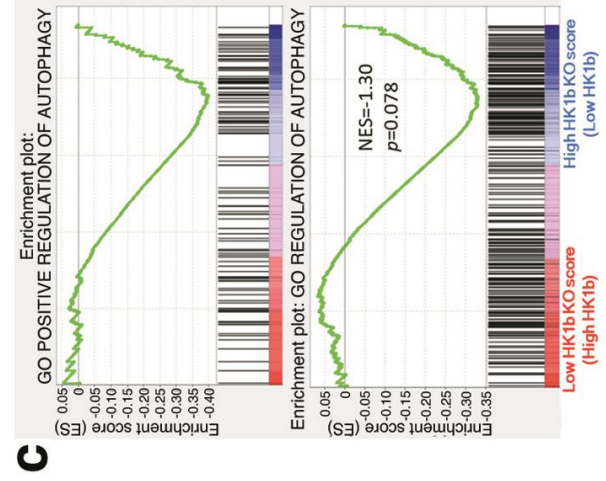
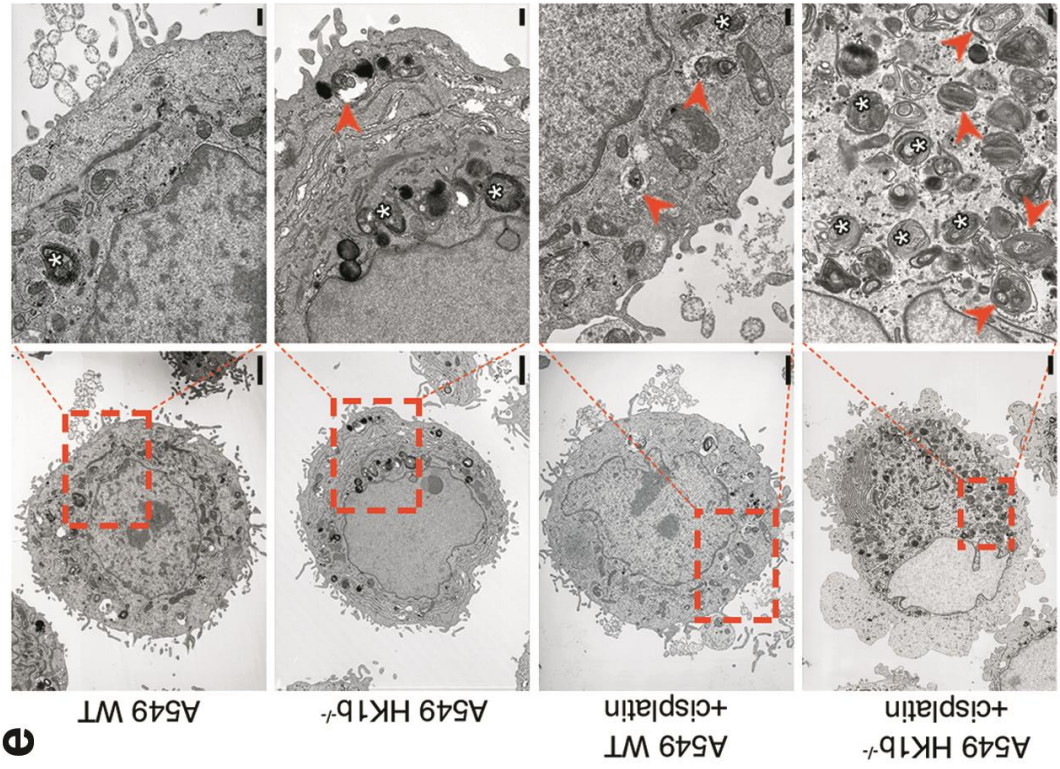
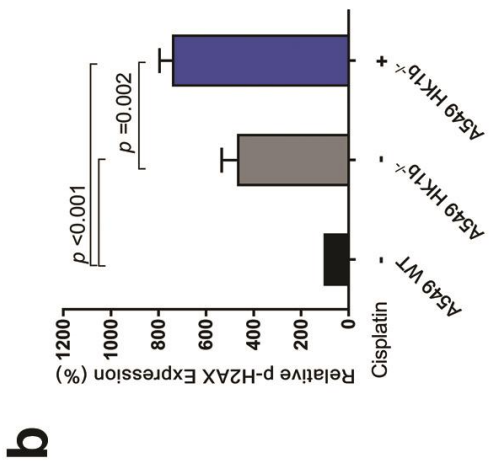
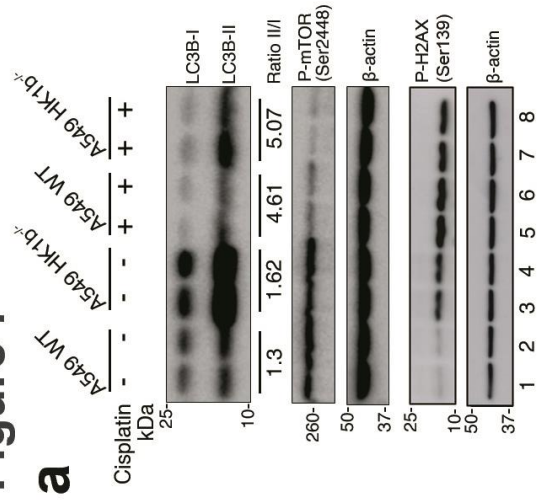
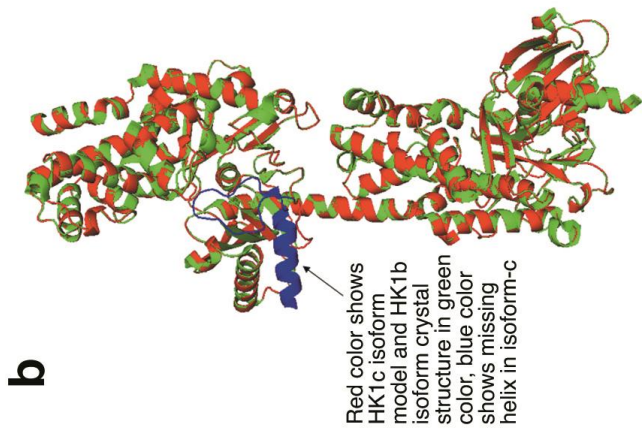
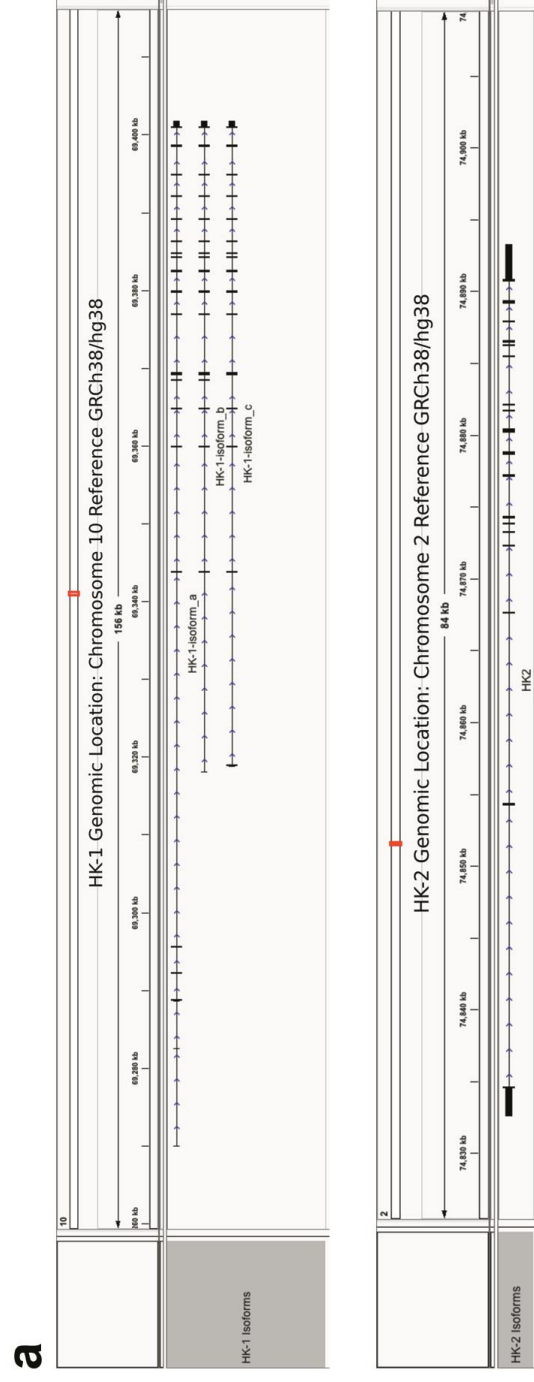


Figure 7

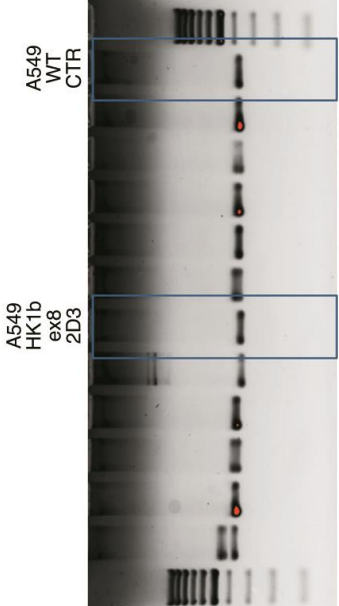
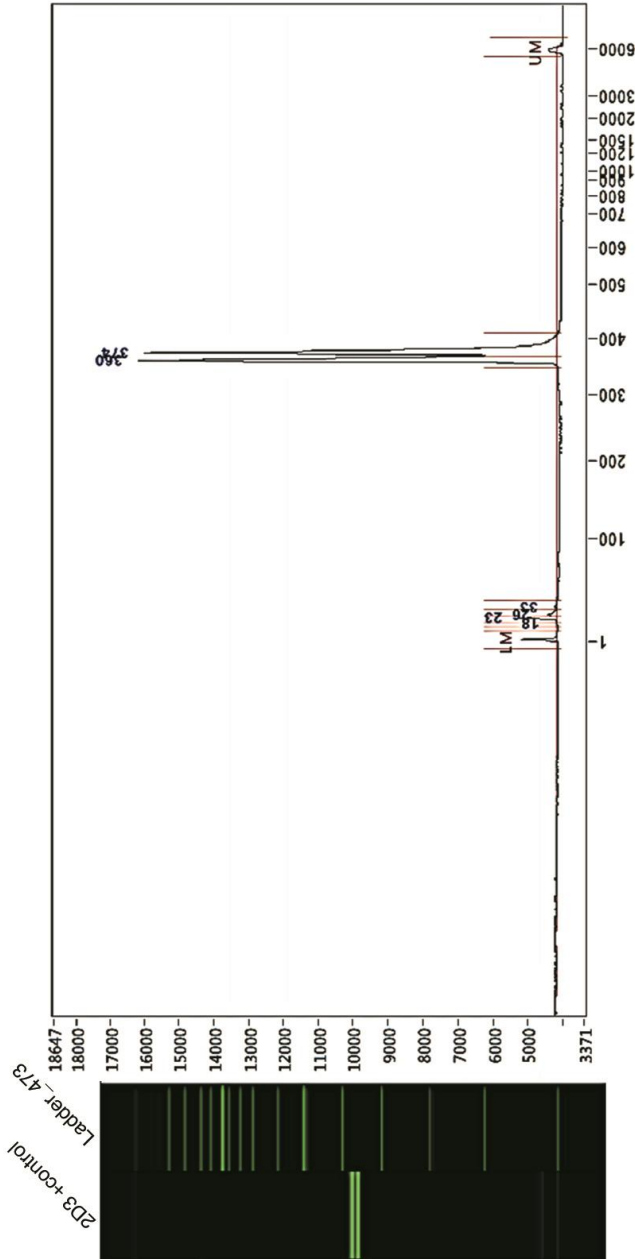


Supplementary Figure 1

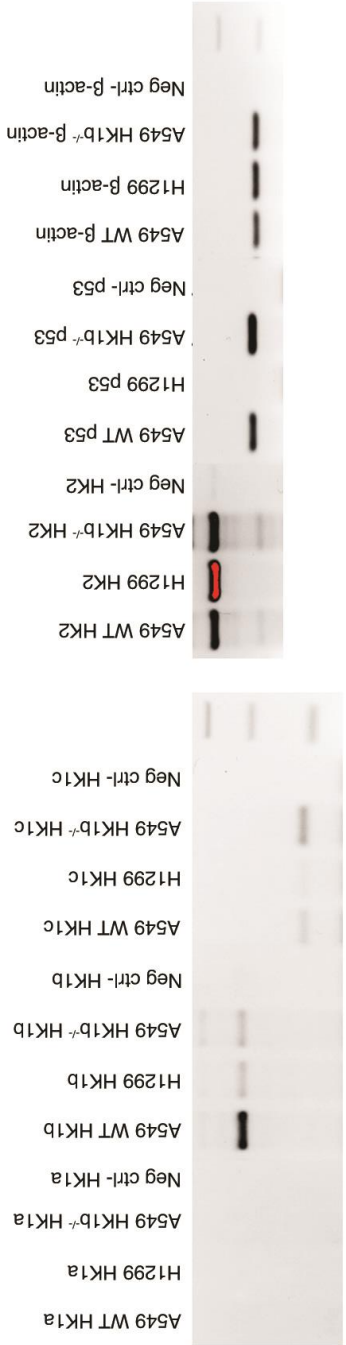


Supplementary Figure 2

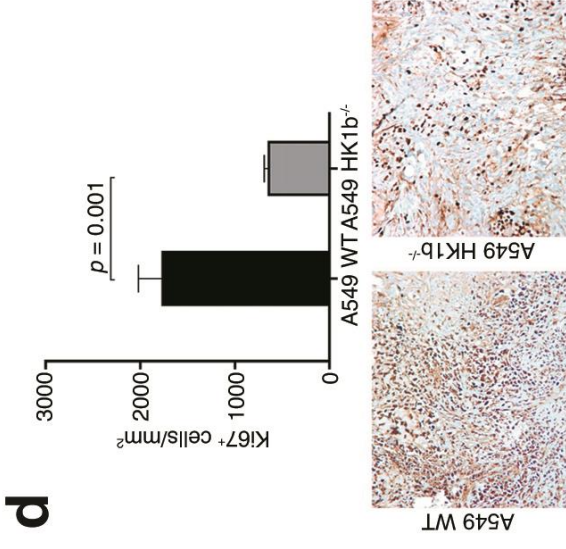
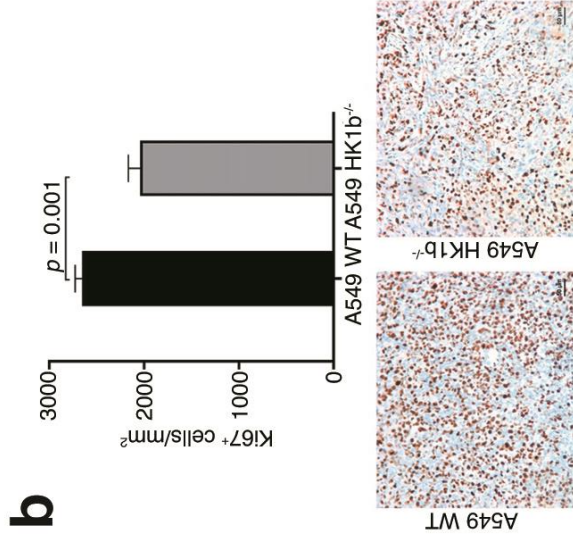
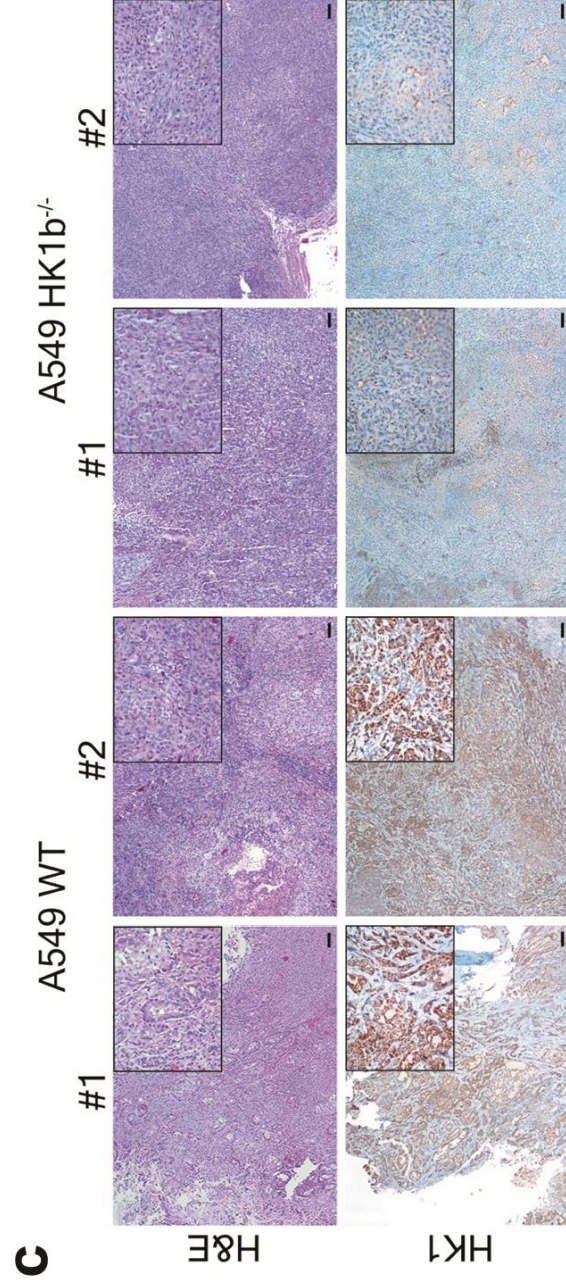
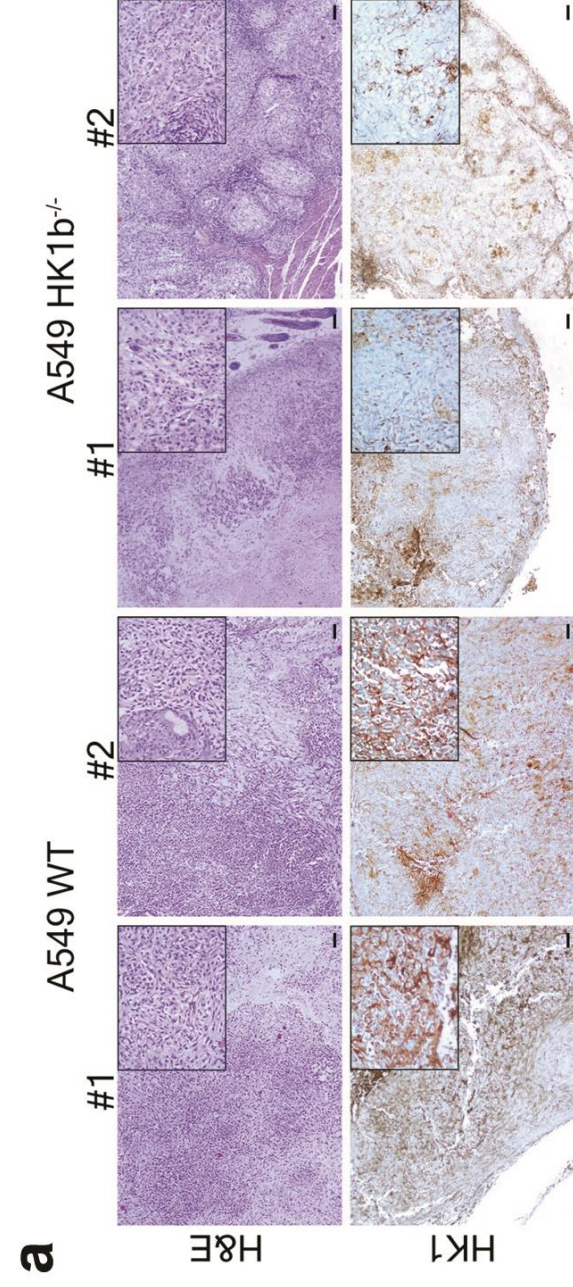
a



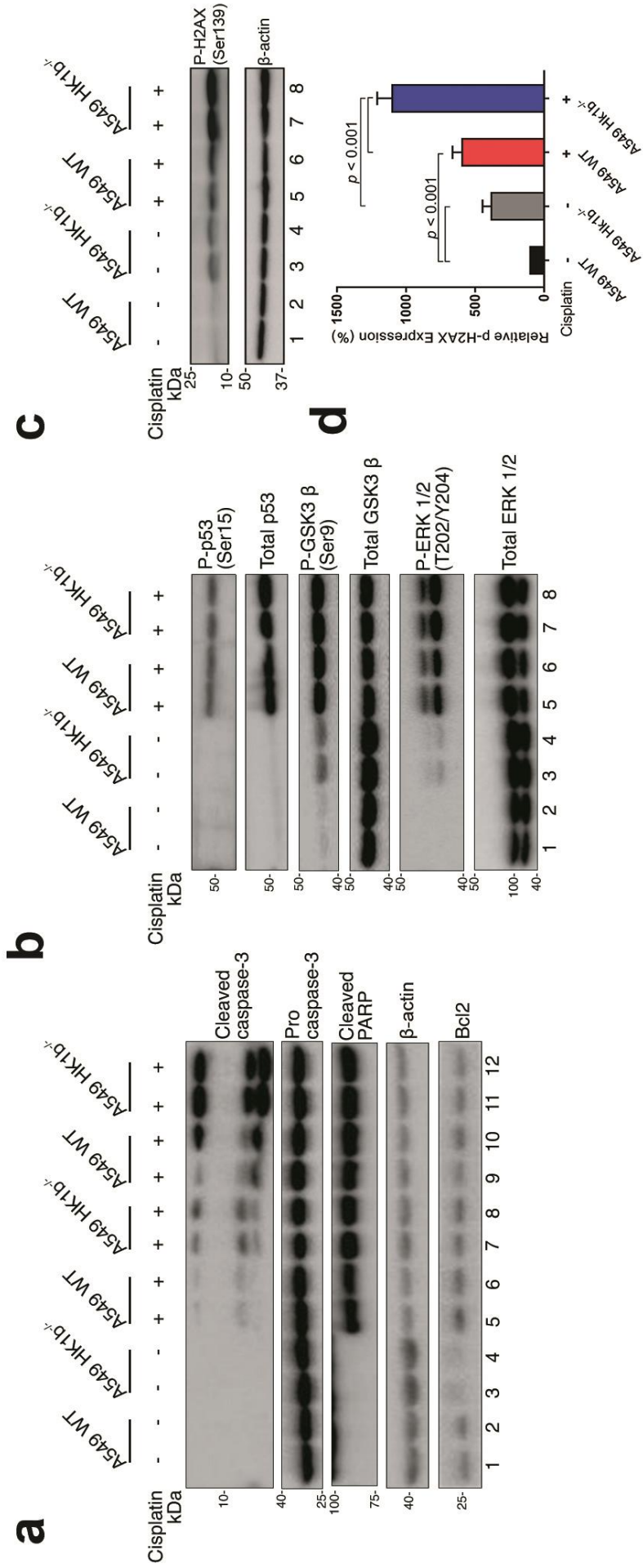
b



Supplementary Figure 3



Supplementary Figure 4



Supplementary Table 1

Patient #	Patient ID	Gender	Age (Years)	Histological type	Grade	Stage	p53	Used in experiment
1	20141-16	Male	64	ADC	2	pT2aN1	pozitif (%95)	WB
2	1103-17	Male	67	ADC	3	pT3N0	negatif (%1)	WB
3	2201-17	Female	75	ADC	2	pT1bN0	negatif (%1)	WB
4	4333-17	Male	68	ADC	3	pT2bN1	pozitif (%90)	WB,q-RT
5	14011-17	Female	53	ADC	1	pT2aN0	negatif (%1)	IHC,WB,q-RT
6	16814-17	Male	54	ADC	3	pT2aN2	negatif (%0)	IHC,WB,q-RT
7	18729-17	Male	54	ADC	3	pT3N0	negatif (%1)	WB,q-RT
8	24555-17	Male	62	Solid ADC	3	ypT2bN0	pozitif (%95)	IHC,WB
9	27384-17	Male	66	Enteric type ADC	2	pT1aN1	negatif (%0)	IHC
10	27796-17	Male	65	Invasive mucinous ADC	1	pT4N1	negatif (%0)	IHC,WB
11	12066-18	Male	66	Enteric type ADC	2	pT2bN0	pozitif (%95)	IHC,WB
12	12867-18	Male	72	Acinar dominant type ADC	2	pT2N1	pozitif (%90)	WB
13	15612-18	Male	68	Solid ADC	3	pT2N1	pozitif (%90)	IHC,WB,q-RT
14	18053-18	Female	76	Acinar dominant type ADC	2	pT2aN0	negatif (%0)	WB,q-RT
15	21673-18	Male	48	Enteric type ADC	2	pT2aN1	negatif (%0)	IHC,WB,q-RT
16	14196-16	Male	62	Basaloid SCC	2	pT3N0	pozitif (%100)	WB,q-RT
17	17682-17	Male	40	SCC	3	pT2aN2	negatif (%1)	WB,q-RT
18	6369-18	Male	69	Solid ADC	3	pT2aN1	negatif (%0)	IHC